LETTER

The centrosome protein AKNA regulates neurogenesis via microtubule organization

Germán Camargo Ortega[1,2,3,22], Sven Falk[1,2,22], Pia A. Johansson[1,2,20,22], Elise Peyre[4], Loïc Broix[4], Sanjeeb Kumar Sahu[5], William Hirst[6,7], Thomas Schlichthaerle[8,9], Camino De Juan Romero[10], Kalina Draganova[1,2], Stanislav Vinopal[11], Kaviya Chinnappa[1,21], Anna Gavranovic[1], Tugay Karakaya[1], Thomas Steininger[1], Juliane Merl-Pham[12], Regina Feederle[13,14], Wei Shao[15,16], Song-Hai Shi[15,16], Stefanie M. Hauck[12], Ralf Jungmann[8,9], Frank Bradke[11], Victor Borrell[10], Arie Geerlof[17], Simone Reber[6,18], Vijay K. Tiwari[5], Wieland B. Huttner[19], Michaela Wilsch-Bräuninger[19], Laurent Nguyen[4] & Magdalena Götz[1,2,8,14]*

The expansion of brain size is accompanied by a relative enlargement of the subventricular zone during development. Epithelial-like neural stem cells divide in the ventricular zone at the ventricles of the embryonic brain, self-renew and generate basal progenitors[1] that delaminate and settle in the subventricular zone in enlarged brain regions[2]. The length of time that cells stay in the subventricular zone is essential for controlling further amplification and fate determination. Here we show that the interphase centrosome protein AKNA has a key role in this process. AKNA localizes at the subdistal appendages of the mother centriole in specific subtypes of neural stem cells, and in almost all basal progenitors. This protein is necessary and sufficient to organize centrosomal microtubules, and promote their nucleation and growth. These features of AKNA are important for mediating the delamination process in the formation of the subventricular zone. Moreover, AKNA regulates the exit from the subventricular zone, which reveals the pivotal role of centrosomal microtubule organization in enabling cells to both enter and remain in the subventricular zone. The epithelial-to-mesenchymal transition is also regulated by AKNA in other epithelial cells, demonstrating its general importance for the control of cell delamination.

We searched the developing mouse cerebral cortex for candidate regulators of SVZ generation and expansion[3–5]. We chose to examine AKNA because levels of *Akna* mRNA correlate with the time at which the subventricular zone (SVZ) is generated (that is, low at embryonic day (E)11, high at E14 and low at E18), and because neural stem cells (NSCs) isolated at the peak of SVZ generation have higher levels of *Akna* when transitioning to basal progenitors[3] (Extended Data Fig. 1a, b). To investigate the function of AKNA, we first generated monoclonal antibodies, which were validated by RNA interference (Extended Data Fig. 1c–f, Methods). Given the annotation of AKNA as an AT-hook transcription factor[6], we were surprised to find specific immunofluorescence signals at centrosomes (Fig. 1a, Extended Data Fig. 1f–m) in different cell types of various species (Extended Data Figs. 1–4, 8, 10), which was confirmed by BAC-transgenic cell lines (Extended Data Fig. 1h) and fractionation of cell lysates (Extended Data Fig. 1n, o). Ultrastructural analysis (Extended Data Fig. 2a–c) showed that AKNA largely localized to the distal part of the subdistal appendages (SDAs)

of the mother centriole in interphase; some AKNA was also found at the proximal ends of centrioles and along microtubules (Extended Data Fig. 2a–d, Supplementary Video 1). Recombinant AKNA protein decorated in vitro-reconstituted microtubules (Extended Data Fig. 2e, Supplementary Video 2). The centrosomal localization of AKNA is not dependent on microtubules or cargo-motors (Extended Data Fig. 2f–h); however, it is dependent on centrioles, as AKNA is absent upon deletion of SAS4[7] (Extended Data Fig. 2i) and the SDA protein ODF2 (Extended Data Fig. 2j, k). AKNA localizes to the centrosome through its carboxyterminal part—a region that was omitted from its first description[6] (see Supplementary Discussion)—as AKNA(1–1080), which lacks the C-terminal 324 amino acids, is distributed in the cytoplasm but is still able to bind to microtubules (Extended Data Fig. 2l–o). Similar to most SDA-associated proteins[8], AKNA dissociates from centrosomes during M-phase without proteolytic degradation (Extended Data Figs. 1h panel 2, 3a, b) and reassembles at the centrosomes during late telophase and early G1 phase (Supplementary Video 3); this dissociation and reassembly is regulated by phosphorylation (Extended Data Fig. 3c, d). Thus, AKNA is a novel integral component of centrosomal SDAs and binding to microtubules, which raises the question of what its role is during development.

AKNA[+] centrosomes showed their highest signal at E14 (compare Fig. 1b with Extended Data Fig. 4a–c), were most frequent in the SVZ (Fig. 1b, Extended Data Fig. 4c), and there was almost no AKNA signal in the cortical plate (in which neurons differentiate). In NSCs at the ventricular surface, only a fraction of centrosomes were AKNA[+] (Fig. 1b, Extended Data Fig. 4d–f). These AKNA[+] centrosomes were in PAX6^{+}TBR2^{+} differentiating NSCs[9], which is consistent with higher levels of *Akna* mRNA in this population[9] (Extended Data Fig. 4g, h). Thus, AKNA exhibits an unprecedented subtype specificity, being restricted to the centrosomes of differentiating NSCs and basal progenitors in forebrain development.

Knockdown of AKNA, mediated by short hairpin (sh)RNA, (Extended Data Fig. 1d) via in utero electroporation (IUE) in E13 cortices led to the retention of GFP^{+} cells in the ventricular zone with more self-renewing (PAX6^{+}TBR2^{−}) NSCs relative to the control conditions, under which many GFP^{+} cells had left the ventricular zone and SVZ by two days post-electroporation (d.p.e.) (Fig. 1c–f,
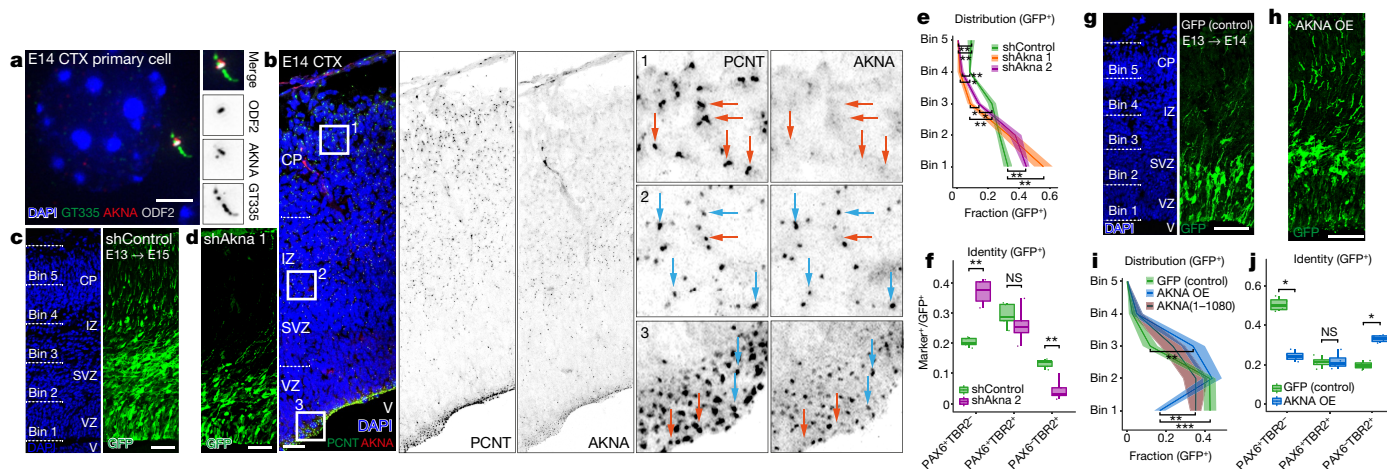
Fig. 1 | AKNA is a centrosome component that regulates NSC delamination. a, Immunostaining of E14 cortex (CTX) cells, showing AKNA at the mother centriole together with ODF2 (distal and subdistal appendages) and GT335 (cilia and centrioles) (*n* = 4). **b**, E14 cortex sections showing AKNA⁺ subsets of centrosomes. Pericentrin⁺ (PCNT⁺) AKNA⁺ centrosomes (blue arrows) at the ventricular zone (VZ) (panel 3); many AKNA⁺ centrosomes in the SVZ and intermediate zone (IZ) (panel 2); and most centrosomes AKNA⁻ (red arrows) in the cortical plate (CP) (panel 1). V, ventricle. *n* = 12. **c, d, g, h**, Confocal micrographs illustrating binning and the distribution of control (**c, g**), *Akna* shRNA no. 1 (shAkna 1) (**d**), electroporated GFP⁺ cells at 2 d.p.e. and AKNA overexpression (OE) at 1 d.p.e. (**h**). **e, f, i, j**, Quantifications as indicated in panels. **e, i**, Mean ± s.e.m. as transparent band in the same colour.

f, j, Box plots show median, quartiles (box) and range (whiskers). **e**, Control shRNA, *n* = 6; *Akna* shRNA no. 1, *n* = 5; *Akna* shRNA no. 2 (shAkna 2), *n* = 5 embryos. *$P \leq 0.05$, **$P \leq 0.01$ (exact *P* values (from top to bottom) 0.00796, 0.00432, 0.00865, 0.02217, 0.03174, 0.01731, 0.00432, 0.00865 and 0.00865). **f**, Control shRNA, *n* = 5; *Akna* shRNA no. 2, *n* = 5 embryos. NS, not significant, **$P \leq 0.01$ (exact *P* values (from left to right) 0.00793, 0.30952 and 0.00793). **i**, GFP (control), *n* = 9; AKNA overexpression, *n* = 11; AKNA(1–1080), *n* = 4 embryos. **$P \leq 0.01$, ***$P \leq 0.001$ (exact *P* values (from top to bottom) 0.00779, 0.00147 and 0.00008). **j**, GFP (control), *n* = 4; AKNA overexpression, *n* = 4 embryos. NS, not significant, *$P \leq 0.05$ (exact *P* values (from left to right), 0.02857, 0.48571 and 0.02857). **e, f, i, j**, Two-sided Mann–Whitney *U* test. Scale bars, 2.5 μm (**a**), 20 μm (**b**), 50 μm (**c, d, g, h**).

Supplementary Video 4). This phenotype was observed with two different shRNAs, was rescued by co-electroporating AKNA (Fig. 1e, Extended Data Fig. 5a, b) and was independent of p53-mediated cell death (Extended Data Fig. 5c–j). Thus, AKNA loss of function impairs NSC delamination, and leads to the retention of more NSCs in the ventricular zone.

Conversely, AKNA overexpression induced a fast delamination, with most GFP⁺ cells being found in the SVZ at 1 d.p.e. (Fig. 1g–i); this resulted in more basal progenitors (PAX6⁻TBR2⁺) and NEUN⁺ neurons and a concomitant decrease in NSCs (PAX6⁺TBR2⁻), as compared to controls (Fig. 1j, Extended Data Fig. 5k). The increased differentiation that occurred upon AKNA overexpression in vivo did
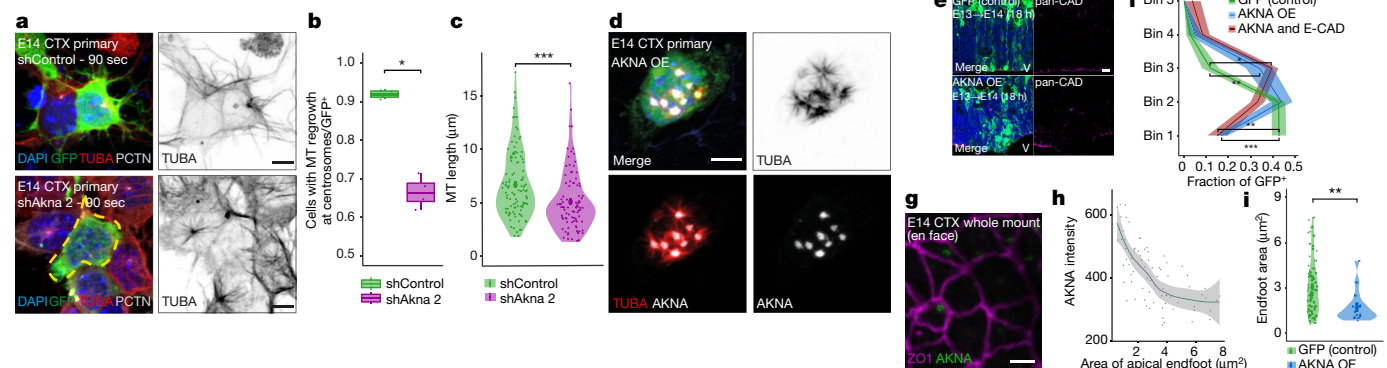

Fig. 2 | AKNA regulates microtubule organization in NSCs. a, Images of E14 cortical cells transfected with shRNA control or *Akna* shRNA no. 2, in nocodazole-based microtubule repolymerization assays. The yellow dashed line indicates a cell in which microtubules did not grow upon AKNA knockdown. **b**, Box plot, median, quartiles (box) and range (whiskers), showing reduced number of cells with centrosomal microtubule (MT) regrowth after AKNA knockdown (shRNA control, *n* = 4; *Akna* shRNA no. 2, *n* = 4 independent experiments, *P* = 0.02857). **c**, Dot and violin plot showing reduced length of microtubule. Dots represent single measurements, mean ± s.e.m in bold in the centre. shRNA control, *n* = 110; *Akna* shRNA no. 2, *n* = 92 microtubule endpoints from 4 independent experiments each (*P* = 0.00007). **d**, AKNA overexpression clusters organize microtubules independently of centrosomes (see also Extended Data Fig. 6b) (*n* = 6). **e**, Most GFP⁺ electroporated cells lose their integration into the apical cadherin belt at the ventricle (V) 18 h after AKNA overexpression (*n* = 3 embryos).

f, Line graph illustrating the distribution of GFP⁺ cells 24 h after IUE. Mean ± s.e.m. as transparent band in the same colour. GFP (control), *n* = 9; AKNA overexpression, *n* = 11; AKNA and E-cadherin (E-CAD) overexpression, *n* = 3 embryos. GFP (control) and AKNA overexpression is based on the same data as shown in Fig. 1i. *$P \leq 0.05$, **$P \leq 0.01$, ***$P \leq 0.001$ (exact *P* values (from top to bottom) 0.02597, 0.00779, 0.00909 and 0.00008). **g, h**, En face view of ventricular endfeet in E14 cortex delineated by ZO-1 (**g**), quantified in **h**, showing the inverse correlation of AKNA immunofluorescence intensity and endfoot size. Transparent band depicts the best-fit curve with the 95% confidence interval (*n* = 76 cells from 4 embryos). **i**, Dot and violin plot (dots represent individual cells, mean ± s.e.m. in bold in the centre) depicting the reduced size of the apical endfeet after AKNA overexpression. GFP (control), *n* = 76 cells; AKNA overexpression, *n* = 14 cells; *n* = 4 embryos each; *P* = 0.00339. **b, c, f, i**, Two-sided Mann–Whitney *U* test. Scale bars, 5 μm.
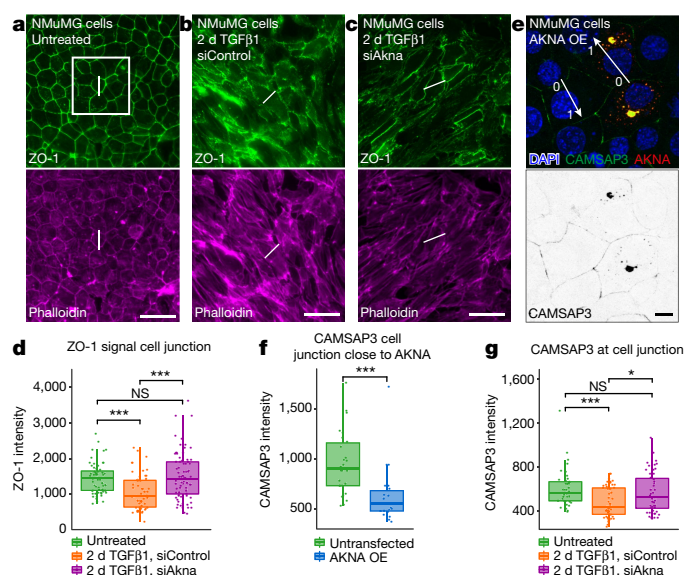
Fig. 3 | EMT progression requires AKNA to dissolve cell junctions.
a–c, Micrographs of NMuMG cells in untreated (**a**) and in TGFβ1-treated, EMT-inducing conditions with control siRNA (siControl) (**b**) or *Akna* siRNA (siAkna) (**c**). ZO-1 is retained at cell junctions, and actin filaments (phalloidin) redistribute less frequently from junctions to cytoplasm, upon AKNA knockdown during EMT. **d**, Dot and box plot showing ZO-1 signal at the cell junction (position 0) (untreated, $n = 60$ cells; TGFβ1-treated and control siRNA, $n = 55$ cells; TGFβ1-treated and *Akna* siRNA, $n = 76$ cells from 3 independent experiments). NS, not significant, $***P \leq 0.001$ (exact P values (from left to right) 5.2×10^{-6}, 0.93189 and 0.00004). **f**, **g**, Dot and box plots showing significant reduction in CAMSAP3 at the cell junction close to AKNA foci after AKNA overexpression (position 1 in the micrograph in **e**) but not in EMT with *Akna* siRNA. In **f**, untransfected, $n = 26$ cells; AKNA overexpression: $n = 22$ cells, from 3 independent experiments. $P = 0.00003$. In **g**, untreated, $n = 42$ cells; TGFβ1-treated and control siRNA, $n = 51$ cells; TGFβ1-treated and *Akna* siRNA, $n = 50$ cells, from 3 independent experiments. NS, not significant, $***P \leq 0.001$ (exact P values (from left to right) 0.00086, 0.75728 and 0.00095). **d**, **f**, **g**, Two-sided Mann–Whitney U test; box plots show median, quartiles (box) and range (whiskers). Scale bars, 10 µm.

not occur in vitro (Extended Data Fig. 5l), and is therefore due to the altered niche that is encountered upon delamination in vivo. Live imaging in cortical slices showed that AKNA overexpression accelerated NSC delamination by a retraction of the apical processes without cell division (28% ($n = 33$) compared to 3% ($n = 165$) in controls) (Supplementary Video 5). Thus, AKNA-induced delamination occurs in interphase, during which AKNA localizes at centrosomes. Consistent with this, overexpression of AKNA(1–1080) hardly increased delamination (Fig. 1i), which indicates the importance of the centrosomal localization of this protein.

Given the function of SDAs[10] in microtubule organization, we tested whether AKNA regulates microtubule organization using nocodazole-based microtubule regrowth assays (Extended Data Fig. 6a). shRNA-mediated AKNA knockdown in primary cortical cells resulted in a significant reduction in the number of cells with centrosomal microtubule regrowth, and of microtubule-fibre length (Fig. 2a–c). Independently of centrosomes, microtubule asters emanated from ectopic AKNA bodies upon AKNA overexpression (Fig. 2d) in an apparently size-dependent manner (Extended Data Fig. 6b). Importantly, AKNA efficiently recruited components of the γ-tubulin ring complex (γTuRC), such as TUBG and GCP4, as well as CKAP5 (also known as ch-TOG) (the mammalian homologue of the microtubule nucleator and polymerase XMAP215[11]), but not other centrosome- and microtubule-associated proteins (Extended Data Fig. 6c, d); this demonstrates the specificity of γTuRC and microtubule nucleation factor recruitment, and how AKNA affects microtubule nucleation and growth. AKNA also recruits and co-immunoprecipitates with SDA

proteins that are involved in microtubule organization such as EB1 (also known as MAPRE1), DCTN1 (also known as P150-Glued), dynein and ODF2[12,13] (Extended Data Fig. 6e, f). AKNA is thus a novel regulator of the centrosome, controlling microtubule organizing centre (MTOC) activity specifically in differentiating NSCs. Notably, AKNA does not affect cilia formation or length in NSCs, despite its localization at SDAs (Extended Data Fig. 7a–d).

Interestingly, CAMSAP3—a microtubule minus-end binding protein—was recruited to AKNA$^+$ foci (Extended Data Fig. 6e). Consistent with CAMSAP proteins anchoring non-centrosomal microtubules at epithelial junctions[14], CAMSAP3 was enriched at the NSC junctions at the ventricular surface (Extended Data Fig. 7e), and cadherin levels at the apical surface were reduced after AKNA overexpression (Fig. 2e). However, maintaining high levels of cadherin with AKNA and E-cadherin co-IUE was not sufficient to interfere with the AKNA-induced delamination process (Fig. 2f). At the junctions surrounding the apical endfoot at the ventricular surface, microtubule and actin belts mediate abscission[15]. High levels of AKNA at the centrosome correlated with a smaller size of apical endfeet, delineated by ZO-1 immunostaining (Fig. 2g, h), and AKNA overexpression increased the number of cells with small endfeet (Fig. 2i). Thus, AKNA regulates the delamination process by increasing centrosomal MTOC activity, weakening junctional complexes and promoting contraction of the apical endfoot.

As AKNA also binds directly to microtubules, we monitored microtubule dynamics by EB3–GFP live imaging in cortex slices after IUE in vivo. EB3–GFP comets grew mostly in a basal direction in NSCs after GFP IUE, as previously shown[16]; however, after AKNA overexpression, comets displayed more random directions (Extended Data Fig. 8a, b, Supplementary Videos 6, 7), which indicates a change in the orientation of microtubule growth and a repositioning of the MTOC toward non-apical positions (see schematic in Extended Data Fig. 7j). AKNA overexpression also had minor effects on the speed of EB3–GFP comets (Extended Data Fig. 8c). To determine possible direct effects of AKNA on microtubules, we reconstituted microtubules in a centrosome-free environment in vitro. The presence of AKNA affected growth velocity but not microtubule lifetime (Extended Data Fig. 8d–f, Supplementary Video 2). Moreover, once a depolymerizing microtubule encountered a site of AKNA enrichment, the depolymerization velocity was significantly reduced (Extended Data Fig. 8g, Supplementary Video 2), which demonstrates that AKNA affects microtubule dynamics in vivo and in vitro. These dynamics are important for delamination, as stabilizing microtubules using Taxol in vivo blocked the AKNA-induced delamination (Extended Data Fig. 8h).

As the delamination from the ventricular zone resembles the epithelial–mesenchymal transition (EMT)[17–19], we asked whether AKNA is more generally relevant for EMT by monitoring normal murine mammary gland (NMuMG) epithelial cells during EMT induced by transforming growth factor beta-1 (TGFβ1)[20,21]. Centrosomal AKNA levels are low in untreated NMuMG cells, but upregulated early in EMT (Extended Data Fig. 8i–k). As expected[14], NMuMG cells show largely non-centrosomal microtubule polymerization before EMT (Supplementary Video 8), and AKNA overexpression increased microtubule nucleation at the centrosome (Extended Data Fig. 8l, Supplementary Video 9). Knockdown of AKNA using small interfering (si)RNAs (Extended Data Fig. 8m) had no effect on the expression of core EMT transcription factors *Twist1*, *Zeb2*, *Snai1* and *Snai2* during EMT (Extended Data Fig. 8i), but led to ZO-1 retention at cell junctions and counteracted the TGFβ1-induced disassembly of these junctions (Fig. 3a–d, Extended Data Fig. 8o, p). AKNA knockdown also attenuated the rearrangement of actin fibres from the junctions to stress fibres (Fig. 3a–c), showing the importance of AKNA in fully dissolving these junctional complexes during EMT. Immunostaining confirmed that AKNA is sufficient to significantly reduce CAMSAP3 at the junctional interface closest to AKNA$^+$ foci upon overexpression, but not CAMSAP3 at more-distant junctions (Fig. 3e, f, Extended Data Fig. 8q). Conversely, AKNA knockdown resulted in the retention of CAMSAP3 at cell junctions after TGFβ1-induced EMT (Fig. 3g, Extended Data
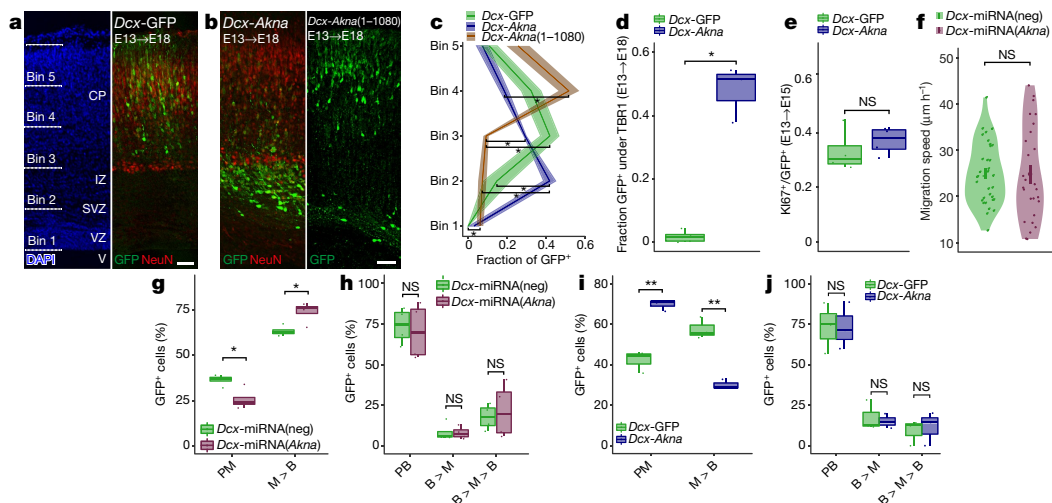
Fig. 4 | AKNA regulates retention of cells within the SVZ. a, b, Confocal micrographs illustrating binning and the distribution of electroporated cells expressing GFP (**a**), *Akna* and GFP, or *Akna*(1–1080) and GFP (**b**) under the control of the *Dcx* promoter at 5 d.p.e. **c,** Line graph illustrating the distribution of GFP⁺ cells after IUE (mean ± s.e.m. as transparent band in the same colour). *Dcx*-GFP, n = 5; *Dcx-Akna*, n = 4; *Dcx-Akna*(1–1080), n = 4 embryos. *P ≤ 0.05 (exact P values (from top to bottom) 0.02857, 0.02857, 0.01587, 0.01587, 0.02857 and 0.01080). **d, e,** Dot and box plots showing the fraction of GFP⁺ cells retained below the cortical plate labelled by TBR1 at 5 d.p.e. (**d,** *Dcx*-GFP, n = 5; *Dcx-Akna*, n = 3 embryos, P = 0.03571) or in cell cycle (KI67⁺) at 2 d.p.e. (**e,** *Dcx*-GFP, n = 4; *Dcx-Akna*, n = 4 embryos; not significant (P = 0.48571). **f,** Dot and violin plot showing the migration speed of control and AKNA-

knockdown neurons in slices at 2 d.p.e. (dots represent individual cells, mean ± s.e.m. in bold) (*Dcx*-miRNA(neg) (sequence predicted not to target any known vertebrate gene), n = 34; *Dcx*-miRNA(*Akna*), n = 26 cells, from 3 independent experiments; not significant (P = 0.67299)). **g–j,** Box plots illustrating the morphological transitions of control and AKNA-knockdown cells (**g, h,** n = 4 embryos each condition) or after AKNA overexpression (**i, j,** n = 3 embryos in each condition). B, bipolar; M, multipolar; PB, persisting bipolar; PM, persisting multipolar. In **g–j,** NS, not significant, *P ≤ 0.05, **P ≤ 0.01. Exact P values (from left to right): 0.02460 and 0.02460 (**g**); 0.75566, 0.93038 and 0.71203 (**h**); 0.00385 and 0.00385 (**i**); 0.99877, 0.71153 and 0.75539 (**j**). **c–f,** Two-sided Mann–Whitney U test; **g–j,** two-sided Student's t-test. Box plots show median, quartiles (box) and range (whiskers). Scale bars, 50 μm.

Fig. 8r). Thus, AKNA mediates the remodelling of junctional complexes by recruiting CAMSAP3 from junctional microtubules to the centrosome, thereby destabilizing junctional cadherins[22] and enabling cells to detach during EMT.

Besides the role of AKNA in the EMT-like delamination of NSCs, we aimed to determine its function within the SVZ, the region with highest levels of AKNA (only 10% of centrosomes were AKNA⁺ above the SVZ in the cortical plate where neurons are located) (Extended Data Fig. 4e). Accordingly, neurons isolated in vitro showed a greater degree of non-centrosomal microtubule polymerization (Extended Data Fig. 9a, b), as compared to NSCs. To counteract the reduction in levels of AKNA above the SVZ, we expressed *Akna* cDNA under the late basal progenitor and neuron-specific doublecortin (*Dcx*) promoter (Extended Data Fig. 9c) at E13. This resulted in many GFP⁺ cells remaining below the cortical plate, as compared to control (Fig. 4a–d), without affecting proliferation at two days post-electroporation (Fig. 4e) or neuronal differentiation (Extended Data Fig. 9d–f). Conversely, *Dcx*-promoter-driven *Akna* microRNAs (miRNAs) did not affect cells that left the SVZ and reached normal positions within the cortical plate, similar to controls (Extended Data Fig. 9g, h). Thus, the downregulation of AKNA that occurs physiologically (Fig. 1b, Extended Data Fig. 4d, e, g) facilitates the transition of neurons from the SVZ to the cortical plate.

To determine at which step AKNA levels are critical in the transition from multipolar SVZ cells to bipolar neurons migrating into the cortical plate[23] (schematic in Extended Data Fig. 7i), we performed live imaging in slices after AKNA overexpression or knockdown in vivo. Control and knockdown cells had similar migratory speeds during locomotion (Fig. 4f), but knockdown cells transitioned faster from the multipolar SVZ morphology to the bipolar morphology of migrating neurons (Fig. 4g, h). Conversely, many cells with AKNA overexpression retained a multipolar morphology and migrated less frequently (Fig. 4i, j, Supplementary Video 10). Thus, AKNA is key not only in bringing cells into the SVZ but also in retaining them there. These data provide further support for the suggestion that the switch to bipolar

morphology and radial neuronal migration requires a switch from a centrosomal to more non-centrosomal MTOC via endogenous down-regulation of AKNA. Indeed, the mutant, non-centrosome-localizing form of AKNA (that is, AKNA(1–1080)) expressed under the *Dcx* promoter failed to retain cells in the SVZ (Fig. 4a–c), which highlights the importance of the centrosomal location of AKNA in this process of morphology switching and migration.

In neurons, microtubules originate preferentially from other non-centrosomal compartments[24], allowing axon and dendrite formation[25,26], and have more stable detyrosinated and acetylated microtubules[27,28]. AKNA counteracts these neuronal hallmarks by promoting centrosomal microtubule nucleation, faster microtubule growth, and more dynamic and less detyrosinated microtubules (Extended Data Fig. 8m, n). Therefore, the downregulation of AKNA is required for neurons to migrate into the cortical plate. Thus, microtubule organization differs profoundly for cell migration into the SVZ, which requires AKNA and a centrosomal MTOC, versus migration out of the SVZ, which requires the loss of AKNA.

During the delamination process, AKNA orchestrates the disassembly of junctional complexes as well as apical endfoot constriction. As microtubule stabilization by Taxol blocked the AKNA-induced delamination, microtubule dynamics and rearrangement are critical. Moreover, the centrosomal localization of AKNA is important, as the non-centrosomal form, AKNA(1–1080), showed impaired delamination but could still bind microtubules. AKNA increased centrosomal microtubule nucleation by recruiting γTuRC and CKAP5[11]. This—together with the low-level direct binding of AKNA to microtubules—explains why AKNA gain of function both promotes nucleation and inhibits depolymerization. AKNA recruits CAMSAP3 to the centrosome. This microtubule minus-end binding protein otherwise tethers microtubules to the adherens junctions[14] contributing to adherens junction stability[22] and cell–cell attachment[29]. Thus, AKNA orchestrates the delamination process by increasing centrosomal microtubule nucleation and recruiting nucleation factors and minus-end stabilizers, thereby destabilizing microtubules at the adherens junctions and

mediating constriction of the apical endfoot. The recruitment of AKNA to the centrosome is post-translationally regulated; SOX4 regulates *Akna* mRNA in EMT[21] and the generation of basal progenitors[30] (Extended Data Fig. 10a–c). Regulating AKNA levels orchestrates delamination and retention in the SVZ—this process is particularly relevant in species with highly proliferative cells[2] in an enlarged SVZ (Extended Data Fig. 10d–r). Thus, the function of AKNA in ontogeny may have profound relevance in phylogeny.

Reporting summary

Further information on research design is available in the Nature Research Reporting Summary linked to this paper.

Data availability

The data generated and analysed in this study are included in the article and its Supplementary Information. Full gel blots can be found in the Extended Data Figures or Supplementary Fig. 1. Any other data in this study are available from the corresponding author upon reasonable request.

Online content

Any methods, additional references, Nature Research reporting summaries, source data, statements of data availability and associated accession codes are available at https://doi.org/10.1038/s41586-019-0962-4.

1. Taverna, E., Götz, M. & Huttner, W. B. The cell biology of neurogenesis: toward an understanding of the development and evolution of the neocortex. *Annu. Rev. Cell Dev. Biol.* **30**, 465–502 (2014).
2. Fernández, V., Llinares-Benadero, C. & Borrell, V. Cerebral cortex expansion and folding: what have we learned? *EMBO J.* **35**, 1021–1044 (2016).
3. Pinto, L. et al. Prospective isolation of functionally distinct radial glial subtypes—lineage and transcriptome analysis. *Mol. Cell. Neurosci.* **38**, 15–42 (2008).
4. Pinto, L. et al. AP2γ regulates basal progenitor fate in a region- and layer-specific manner in the developing cortex. *Nat. Neurosci.* **12**, 1229–1237 (2009).
5. Stahl, R. et al. Trnp1 regulates expansion and folding of the mammalian cerebral cortex by control of radial glial fate. *Cell* **153**, 535–549 (2013).
6. Siddiqa, A. et al. Regulation of CD40 and CD40 ligand by the AT-hook transcription factor AKNA. *Nature* **410**, 383–387 (2001).
7. Insolera, R., Bazzi, H., Shao, W., Anderson, K. V. & Shi, S. H. Cortical neurogenesis in the absence of centrioles. *Nat. Neurosci.* **17**, 1528–1535 (2014).
8. Nigg, E. A. & Stearns, T. The centrosome cycle: centriole biogenesis, duplication and inherent asymmetries. *Nat. Cell Biol.* **13**, 1154–1160 (2011).
9. Aprea, J. et al. Transcriptome sequencing during mouse brain development identifies long non-coding RNAs functionally involved in neurogenic commitment. *EMBO J.* **32**, 3145–3160 (2013).
10. Uzbekov, R. & Alieva, I. Who are you, subdistal appendages of centriole? *Open Biol.* **8**, 180062 (2018).
11. Thawani, A., Kadzik, R. S. & Petry, S. XMAP215 is a microtubule nucleation factor that functions synergistically with the γ-tubulin ring complex. *Nat. Cell Biol.* **20**, 575–585 (2018).
12. Askham, J. M., Vaughan, K. T., Goodson, H. V. & Morrison, E. E. Evidence that an interaction between EB1 and p150^Glued is required for the formation and maintenance of a radial microtubule array anchored at the centrosome. *Mol. Biol. Cell* **13**, 3627–3645 (2002).
13. Ibi, M. et al. Trichoplein controls microtubule anchoring at the centrosome by binding to Odf2 and ninein. *J. Cell Sci.* **124**, 857–864 (2011).
14. Tanaka, N., Meng, W., Nagae, S. & Takeichi, M. Nezha/CAMSAP3 and CAMSAP2 cooperate in epithelial-specific organization of noncentrosomal microtubules. *Proc. Natl Acad. Sci. USA* **109**, 20029–20034 (2012).
15. Kasioulis, I., Das, R. M. & Storey, K. G. Inter-dependent apical microtubule and actin dynamics orchestrate centrosome retention and neuronal delamination. *eLife* **6**, e26215 (2017).
16. Tsai, J. W., Lian, W. N., Kemal, S., Kriegstein, A. R. & Vallee, R. B. Kinesin 3 and cytoplasmic dynein mediate interkinetic nuclear migration in neural stem cells. *Nat. Neurosci.* **13**, 1463–1471 (2010).
17. Itoh, Y. et al. Scratch regulates neuronal migration onset via an epithelial–mesenchymal transition-like mechanism. *Nat. Neurosci.* **16**, 416–425 (2013).
18. Zander, M. A., Burns, S. E., Yang, G., Kaplan, D. R. & Miller, F. D. Snail coordinately regulates downstream pathways to control multiple aspects of mammalian neural precursor development. *J. Neurosci.* **34**, 5164–5175 (2014).
19. Singh, S. et al. Zeb1 controls neuron differentiation and germinal zone exit by a mesenchymal–epithelial-like transition. *eLife* **5**, e12717 (2016).
20. Sahu, S. K. et al. JNK-dependent gene regulatory circuitry governs mesenchymal fate. *EMBO J.* **34**, 2162–2181 (2015).
21. Tiwari, N. et al. Sox4 is a master regulator of epithelial-mesenchymal transition by controlling Ezh2 expression and epigenetic reprogramming. *Cancer Cell* **23**, 768–783 (2013).
22. Meng, W., Mushika, Y., Ichii, T. & Takeichi, M. Anchorage of microtubule minus ends to adherens junctions regulates epithelial cell–cell contacts. *Cell* **135**, 948–959 (2008).
23. Cooper, J. A. Molecules and mechanisms that regulate multipolar migration in the intermediate zone. *Front. Cell. Neurosci.* **8**, 386 (2014).
24. Petry, S. & Vale, R. D. Microtubule nucleation at the centrosome and beyond. *Nat. Cell Biol.* **17**, 1089–1093 (2015).
25. Stiess, M. et al. Axon extension occurs independently of centrosomal microtubule nucleation. *Science* **327**, 704–707 (2010).
26. Sakakibara, A. et al. Dynamics of centrosome translocation and microtubule organization in neocortical neurons during distinct modes of polarization. *Cereb. Cortex* **24**, 1301–1310 (2014).
27. Aillaud, C. et al. Vasohibins/SVBP are tubulin carboxypeptidases (TCPs) that regulate neuron differentiation. *Science* **358**, 1448–1453 (2017).
28. Song, Y. & Brady, S. T. Post-translational modifications of tubulin: pathways to functional diversity of microtubules. *Trends Cell Biol.* **25**, 125–136 (2015).
29. Pongrakhananon, V., Wattanathamsan, O., Takeichi, M., Chetprayoon, P. & Chanvorachote, P. Loss of CAMSAP3 promotes EMT via the modification of microtubule–Akt machinery. *J. Cell Sci.* **131**, jcs216168 (2018).
30. Chen, C., Lee, G. A., Pourmorady, A., Sock, E. & Donoghue, M. J. Orchestration of neuronal differentiation and progenitor pool expansion in the developing cortex by SoxC genes. *J. Neurosci.* **35**, 10629–10642 (2015).

Extended Data Fig. 1 | See next page for caption.

Extended Data Fig. 1 | AKNA expression, centrosome localization and antibody verification. a, Quantitative PCR with reverse transcription (RT-qPCR) data show higher levels of *Akna* mRNA in E14 cerebral cortex than in E11 or E18 cerebral cortex ($n = 3$ biologically independent samples, mean ± s.e.m., one-way ANOVA with Tukey's post hoc test. **b**, Microarray data depicting higher expression of AKNA in NSCs that generate basal progenitors (CD133^{+}, hGFAP–GFP^{high} (transgenic mice expressing GFP under control of the human GFAP promoter)[3] (hGFAP–GFP, $n = 4$; hGFAP-GFP^{low}, $n = 3$ independent samples, mean ± s.e.m., two-sided Student's *t*-test, note that all GFAP–GFP^{+} cells were double-stained for CD133 prior to FACS (see ref. [3]). **c**, Western blot of AKNA in E14 cerebral cortex lysate running at a higher-than-predicted (153 kDa) molecular mass, owing to phosphorylation (data not shown, see also Extended Data Fig. 3d) ($n = 8$ independent experiments). **d**, **e**, Western blot of AKNA in Neuro2a cell lysates after transfection with *Akna* shRNA no. 1, *Akna* shRNA no. 2 or control shRNA (**d**, $n = 2$ independent experiments) or 3 different miRNAs and control (**e**, 1 experiment), using the antibody clone 14D7. **f**, AKNA immunofluorescence using clone 25F1 in primary E14 cortical cells, which show TBR2^{+} basal progenitors that lack AKNA immunofluorescence signal upon transfection with *Akna* siRNAs but not with control siRNA, demonstrating the specificity of the immunostaining ($n = 3$ independent experiments). **g**, Immunofluorescence of AKNA and TUBG in primary E14 cortical cells, showing AKNA signal surrounding a single TUBG[+] centriole ($n > 10$ independent experiments). **h**, A20 BAC transgenic cell line showing GFP-tagged AKNA at centrosomes marked by TUBG in interphase (**h′** and **h‴**) but not during mitosis (**h″**) ($n = 3$ independent experiments). **i**, Predicted domains of mouse AKNA protein. **j**, Amino acid sequence of AT-hook-containing transcription-factor domain of AKNA, and of the AT-hook-like domain. Note that AKNA lacks the GRP core sequence surrounded by several K and R amino acids, which is required for DNA- or RNA-binding AT-hook domains (such as the AT-hook domains of HMGA1). **k**–**m**, Immunostaining of dissociated cerebral organoid cells derived from human induced pluripotent stem cells (hiPSCs), showing AKNA localization at centrosomes with 3 different monoclonal antibodies ($n = 2$ independent experiments each). Clone 9G1 and 4F5 recognize epitopes in the N- and C-terminal parts of the protein, respectively, which suggests that different splice variants[6,31] still localize at centrosomes. One (mother) centriole is enriched for AKNA. **n**, Western blot of AKNA in nuclear and cytoplasmic cell fractions of A20 cells, showing AKNA signal in the cytoplasm only ($n = 2$ independent experiments). **o**, Mass spectrometric analysis of sucrose-gradient-based isolated cellular sub-fractions of A20 cells. AKNA is enriched in fractions 3 and 4, which contain the centrosomal components listed on the right side (1 experiment). Scale bars, 5 μm (**f**, **h**, **k**–**m**), 2.5 μm (**g**).

31. Sims-Mourtada, J. C. et al. The human AKNA gene expresses multiple transcripts and protein isoforms as a result of alternative promoter usage, splicing, and polyadenylation. *DNA Cell Biol.* **24**, 325–338 (2005).
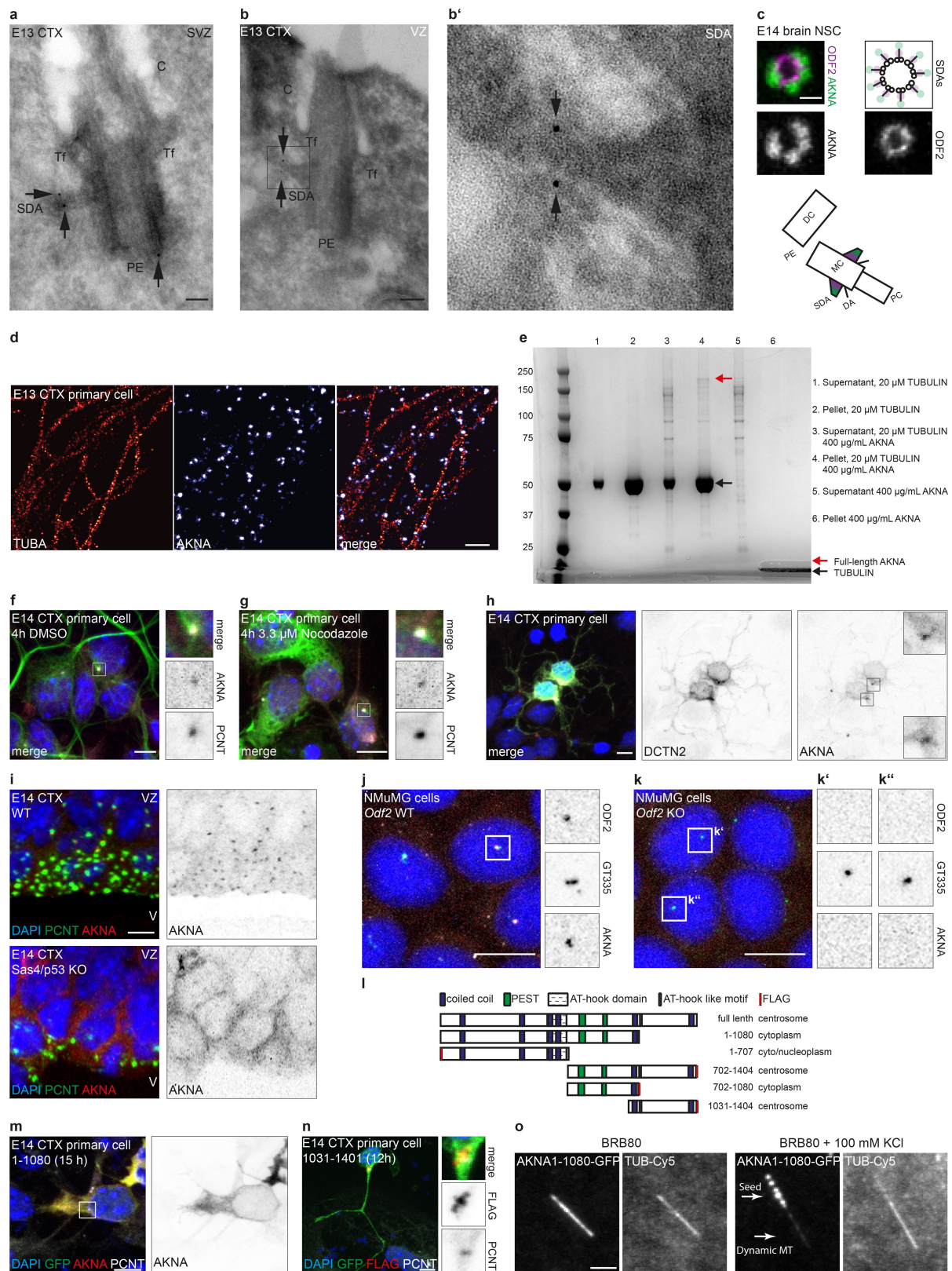
Extended Data Fig. 2 | See next page for caption.

**Extended Data Fig. 2 | Mechanisms of AKNA localization.**
a, **b**, Electron microscopy micrographs showing AKNA immunogold-labelling at SDAs in the SVZ (**a**) and ventricular zone (**b**) of E13 cerebral cortex sections; **b′**, a magnification of the boxed area showing an SDA in **b** ($n = 3$ embryos). **c**, Stimulated emission depletion nanoscopy image showing AKNA immunofluorescence signal surrounding ODF2 immunofluorescence signal; this reveals the more-distal localization of AKNA at the SDA, as compared to ODF2, which localizes proximally with respect to the centriole in E14 brain NSCs (summarized in the schematic below; AKNA, green, ODF2, magenta) ($n = 2$ independent experiments). **d**, Micrographs showing DNA points accumulation for imaging in nanoscale topography super-resolution images of AKNA and TUBA, illustrating that AKNA is present along microtubules in E14 cortical cells ($n = 3$ independent experiments). **e**, Coomassie staining of a sodium dodecyl sulfate polyacrylamide gel electrophoresis (SDS–PAGE) gel showing samples of purified in vitro polymerized tubulin, with and without addition of purified recombinant AKNA as indicated ($n = 2$ independent experiments). Note that full-length AKNA co-precipitates with polymerized tubulin (lane 4), showing that AKNA is able to bind microtubules in vitro. **f–h**, E14 primary cortical cells treated with DMSO (**f**), nocodazole (**g**) or DCTN2 overexpression (**h**) show AKNA immunofluorescence remaining at centrosomes after microtubule depolymerization ($n = 4$ (**f**, **g**) and 3 (**h**) independent experiments). **i**, Micrographs showing AKNA immunofluorescence signal at centrosomes at the apical, ventricular surface in sections of E14 wild-type, but not

$Sas4^{-/-}p53^{-/-}$ ($Sas4$ is also known as $Cenpji$, and $p53$ is also known as $Trp53$) mice that lack centrioles[7] ($n = 2$ independent experiments). Note that PCNT$^+$ pericentriolar material is present in the absence of centrioles in $Sas4^{-/-}p53^{-/-}$ mice. **j**, **k**, AKNA immunofluorescence of wild-type (**j**) or CRISPR–Cas9-generated $Odf2$ knock-out (**k**) mammary epithelial cells, showing that AKNA is lost from centrioles lacking SDAs ($n = 3$ independent experiments each). **l**, Schematic of different truncated AKNA variants used to analyse sub-cellular localization, as indicated to the right. **m**, **n**, Micrographs showing examples of the localization of truncated AKNA forms expressed in primary E14 cortical cells. Constructs containing the last 370 amino acids (**n**) localize to centrosomes, whereas AKNA(1–1080) is not localized at the centrosome (square) and is mainly cytoplasmic (**m**) ($n = 3$ independent experiments each). Notably, the clone used[6] to first characterize AKNA lacked the C-terminal centrosome-targeting part. **o**, Representative images obtained from total internal reflection fluorescence (TIRF) time-lapse recordings of microtubules assembled in vitro from bovine brain tubulin, labelled with Cy5 in the presence of AKNA(1–1080)–GFP. BRB80 buffer with high salt concentration (100 mM KCl) was used to rule out unspecific binding to microtubules ($n = 2$ independent experiments). These data demonstrate that AKNA is an integral component of SDAs, is able to bind microtubules and is not recruited to centrosomes by microtubule or dynein–dynactin motors. Scale bars, 0.1 μm (**a–c**), 2 μm (**d**), 3 μm (**o**), 5 μm (**f–h**, **m**), 10 μm (**i–k**, **n**).
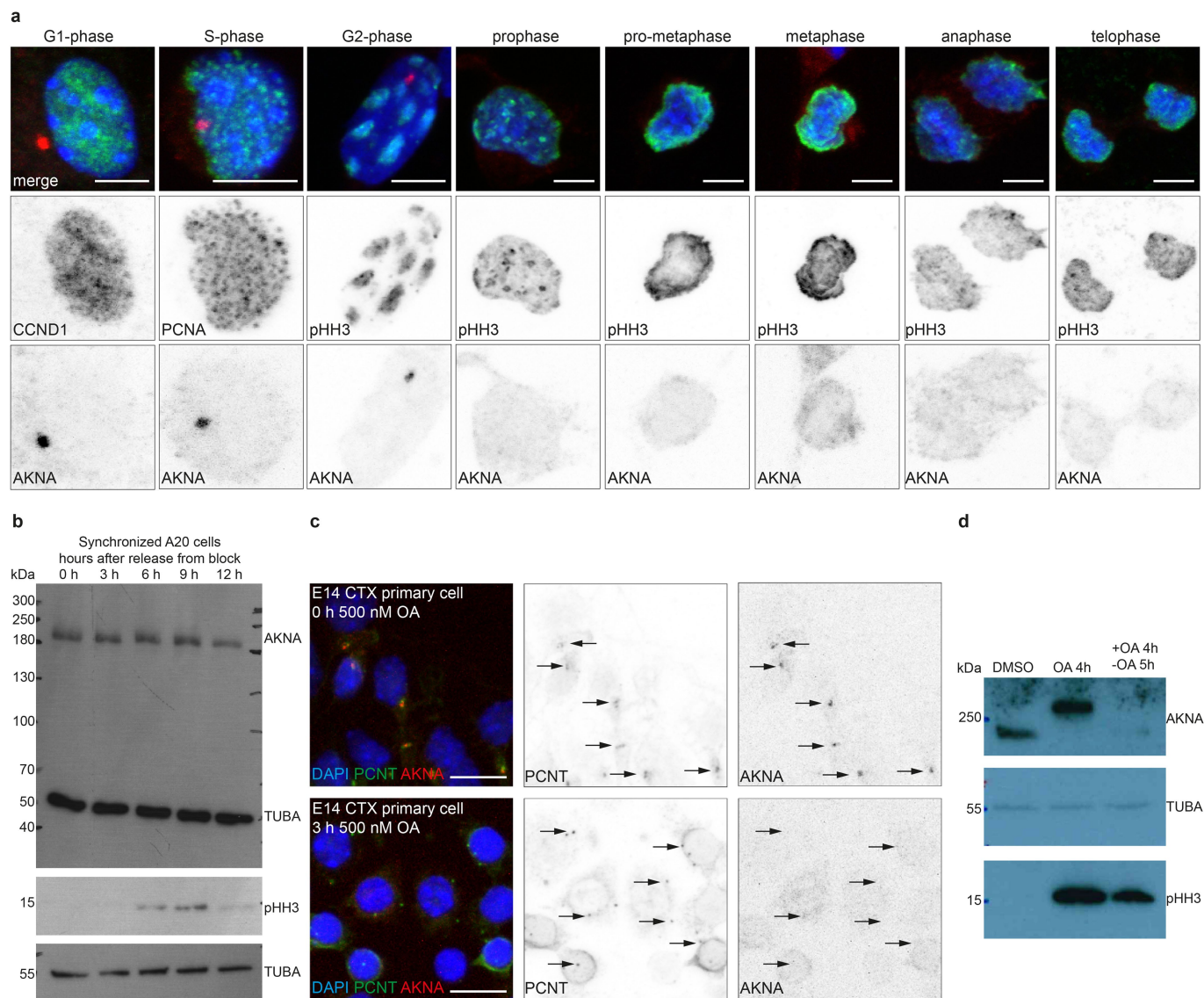
Extended Data Fig. 3 | AKNA dissociates from the centrosome during mitosis and upon increased phosphorylation. a, Immunofluorescence of AKNA in primary E14 cortical cells at different phases of the cell cycle, showing the lack of AKNA immunofluorescence at the centrosome during mitosis ($n = 3$ independent experiments). **b**, Western blot of AKNA in synchronized A20 cells, showing that AKNA protein is not degraded during mitosis (as indicated by the presence of phospho-histone H3) ($n = 2$ independent experiments). **c**, Representative micrographs of AKNA and PCNT immunofluorescence in E14 primary cortical cells treated with 500 nM okadaic acid (OA). Note that AKNA immunofluorescence is observed at centrosomes at 0 h but is undetectable in most cells 3 h after treatment, which shows that the centrosomal localization of AKNA is phosphorylation-dependent ($n = 3$ independent experiments). **d**, Western blot of lysates of OA-treated cells shows that phosphorylation—here caused by protein phosphatase inhibition—shifts that AKNA band on SDS–PAGE, and subsequently leads to protein degradation as observed in lysates of cells 5 h after OA washout ($n = 3$ independent experiments). Scale bars, 5 μm (**a**), 10 μm (**c**).
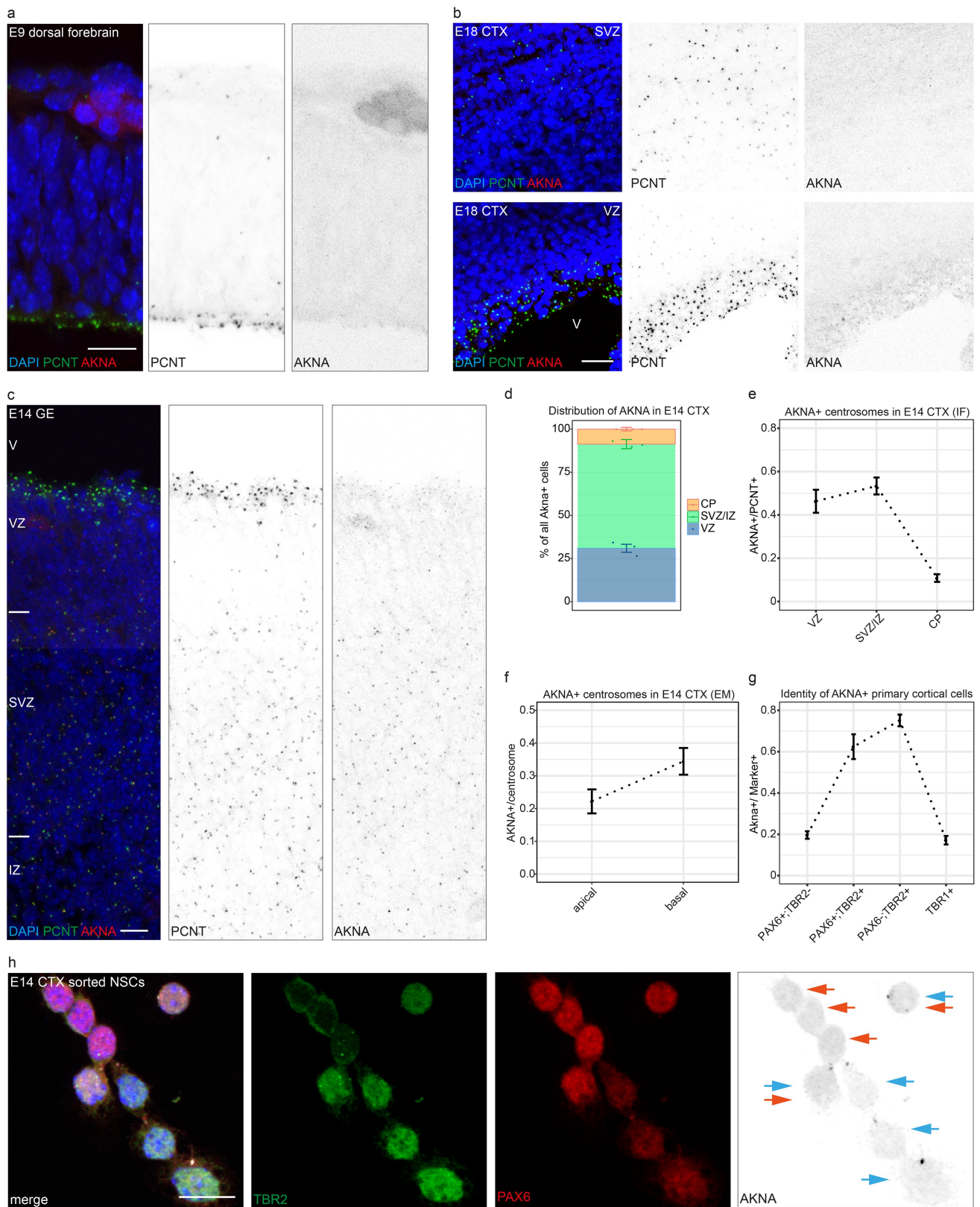
Extended Data Fig. 4 | See next page for caption.

Extended Data Fig. 4 | Temporal and sub-type-specific regulation of AKNA in the developing telencephalon. a–c, Micrographs showing that PCNT$^+$ centrosomes lack AKNA in the cerebral cortex at E9 (**a**, $n = 2$ experiments) and E18 (**b**, $n = 2$ experiments), whereas AKNA is enriched in the ventricular zone and—specifically—the SVZ at E14 in the ganglionic eminence (**c**, $n > 10$ experiments) and the cerebral cortex (Fig. 1). **d**, Distribution of AKNA$^+$ centrosomes in the E14 cortex ($n = 3$ independent experiments). **e–g**, Plots showing the percentage of AKNA$^+$ centrosomes in E14 and E13 cerebral cortex regions as indicated (**e**, **f**, $n = 3$ independent experiments), and in dissociated primary E14 cortical cells (**g**), which reveals that cells with AKNA$^+$ centrosomes are mostly differentiating NSCs (PAX6$^+$TBR2$^+$) and PAX6$^-$TBR2$^+$ basal progenitors ($n = 3$ independent experiments). EM, electron microscopy; IF, immunofluorescence. **h**, Micrographs of cells isolated from E14 cerebral cortex by FACS using prominin 1, and stained for PAX6 (red arrows) and TBR2 (blue arrows). This shows that double-positive (differentiating) NSCs have AKNA$^+$ centrosomes, whereas PAX6$^+$TBR2$^-$ (proliferating) NSCs do not ($n = 2$ experiments). Data in **d–g** are presented as mean $\pm$ s.e.m. Scale bars, 10 μm (**a**, **c**, **h**), 20 μm (**b**).
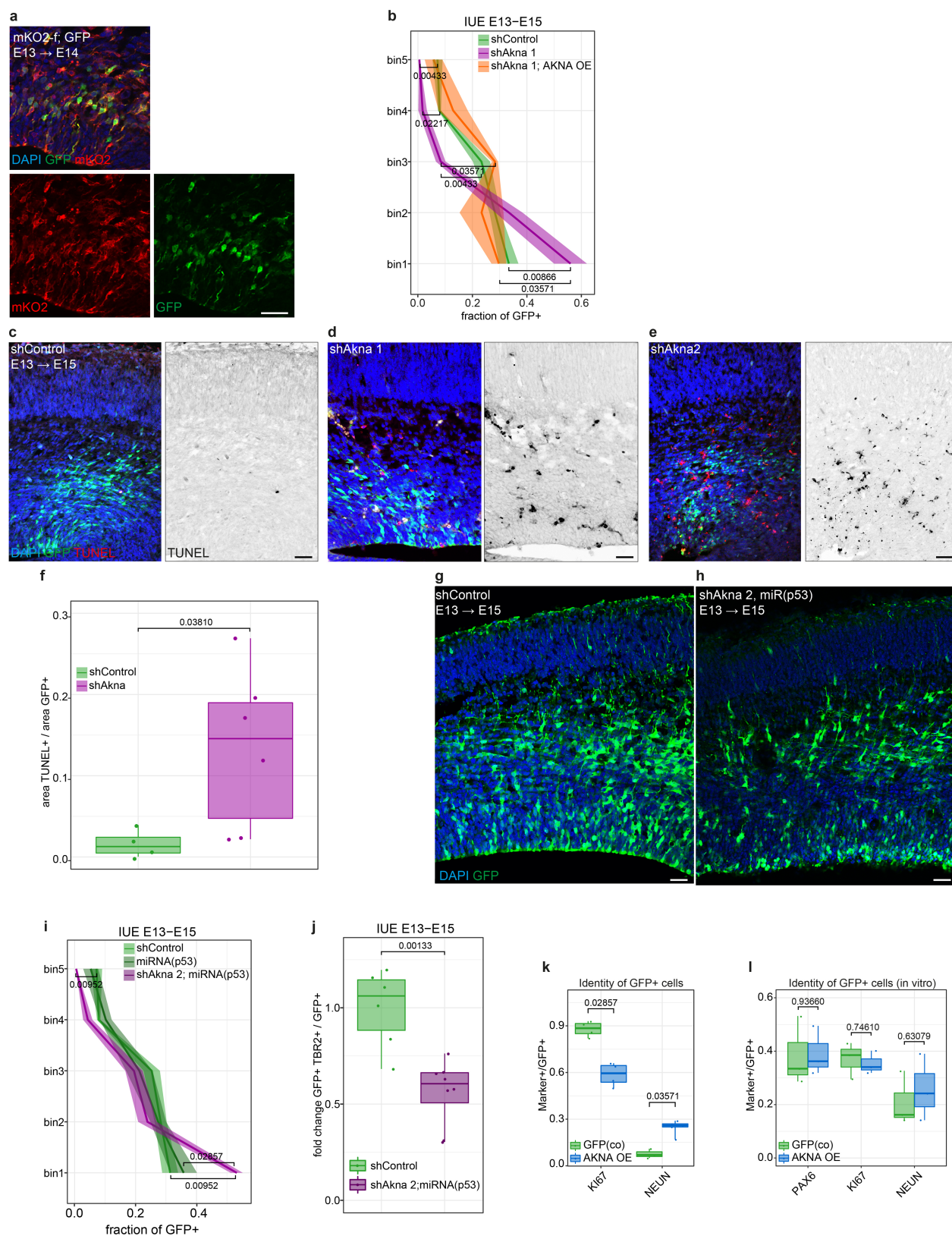
Extended Data Fig. 5 | See next page for caption.

Extended Data Fig. 5 | AKNA knock down elicits cell death, and delamination defects persist upon cell-death rescue by p53 reduction.
a, Confocal micrographs showing staining of E14 cortex one day after co-IUE of membrane-tagged mKO2 (monomeric Kusabira-Orange2) and cytoplasmic GFP. Note that the vast majority of cells electroporated with one plasmid also express the marker of the second plasmid ($n = 4$ embryos). **b**, Line graph illustrating the distribution of GFP$^+$ cells in the cerebral cortex after IUE for control shRNA ($n = 6$ embryos), *Akna* shRNA no. 1 ($n = 5$ embryos) and co-IUE of *Akna* shRNA and AKNA overexpression ($0.2\ \mu g\ \mu l^{-1}$) ($n = 3$ embryos). Note that the effect of AKNA knockdown is rescued with the appropriate amount of *Akna* expression, and is therefore specific. **c–e**, Micrographs showing TUNEL staining in E15 cerebral cortex, indicating cell death two days after IUE with *Akna* shRNA no. 1 (**d**, $n = 3$ embryos) or *Akna* shRNA no. 2 (**d**, $n = 3$ embryos) but not with control plasmids (**c**, $n = 4$ embryos). **f**, Dot and box plot showing the TUNEL$^+$ area per electroporated (GFP$^+$) area with control shRNA ($n = 4$ embryos) and *Akna* shRNA ($n = 6$ embryos, *Akna* shRNA no. 1 and *Akna* sRNA no. 2). **g, h**, Micrographs showing the distribution of GFP$^+$ cells in E15 cerebral cortex two days after IUE with control shRNA (**g**) or *Akna* shRNA no. 2 plus *p53* miRNA plasmids (**h**). Note that p53 downregulation rescues the apoptotic effect

of AKNA knockdown. **i**, Line graph illustrating the distribution of GFP$^+$ cells in the cerebral cortex after control shRNA ($n = 6$ embryos), *p53* miRNA ($n = 4$ embryos), and *Akna* shRNA no. 2 and *p53* miRNA ($n = 4$, embryos) IUE, showing the delamination defect that occurs upon AKNA knockdown is also present when apoptosis is blocked (*Akna* shRNA no. 2 and *p53* miRNA). Note that p53 knockdown on its own does not alter the distribution of GFP$^+$ cells. **j**, Dot and box plot showing the decrease of GFP$^+$TBR2$^+$ cells after IUE of *Akna* shRNA-positive, *p53* miRNA, as compared to control; this shows that defects in delamination are accompanied by retaining an NSC fate (control shRNA, $n = 6$; *Akna* shRNA no. 2 and *p53* miRNA, $n = 8$ embryos). **k**, Dot and box plot showing a decrease in proliferating (KI67$^+$, $n = 4$ embryos each), and a concomitant increase in differentiated, NEUN$^+$ cells analysed at E14 after IUE at E13 (GFP, $n = 3$; AKNA overexpression, $n = 5$ embryos). **l**, Box plot showing the fraction of PAX6$^+$, KI67$^+$ and NEUN$^+$ in E14 primary cortical cells 48 h after transfection in vitro ($n = 3$ embryos each). **b, i**, Line graphs show mean $\pm$ s.e.m. as a transparent band in the same colour; control shRNA and *Akna* shRNA no. 1 data in **b** and control shRNA in **i** are the same data as shown in Fig. 1e. Box plots show median, quartiles (box) and range (whiskers); **b, f, i–k**, two-sided Mann–Whitney U test; **l**, two-sided Students t-test. Scale bars, $50\ \mu m$.
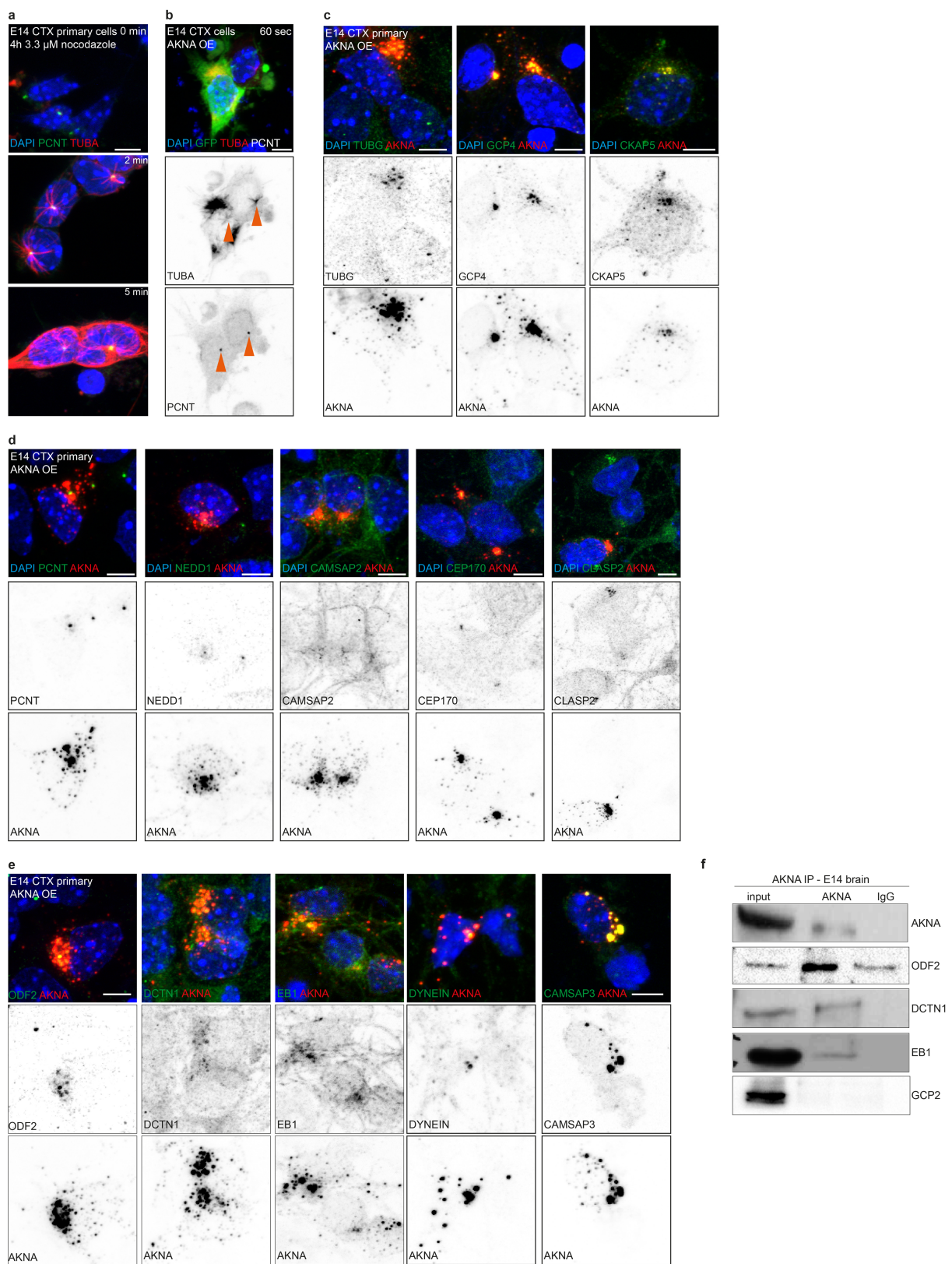
Extended Data Fig. 6 | See next page for caption.

Extended Data Fig. 6 | AKNA is sufficient to mediate microtubule polymerization and recruit γTuRC, CKAP5 and SDA components.
a–e, Micrographs of E14 primary cortex cells treated and immunostained as indicated. **a**, Time series depicting regrowth of the microtubule cytoskeleton after nocodazole-mediated depolymerization ($n = 3$ experiments). **b**, Regrowth of the microtubules 60 s after nocodazole-mediated depolymerization in AKNA overexpression (GFP$^+$) cells ($n > 10$ experiments). Red arrows indicate centrosomes. Note that microtubules polymerize also from ectopic AKNA$^+$ sites. **c**, Confocal images showing co-labelling of AKNA foci with the γTuRC components TUBG and GCP4, and microtubule nucleation factor CKAP5 ($n = 2$ experiments).

d, Confocal micrographs illustrating that AKNA foci fail to recruit PCNT, NEDD1 and the microtubule minus-end capping-proteins CAMSAP2, CEP170 and CLASP2 ($n = 2$ experiments). **e**, Confocal micrographs depicting co-localization of ectopic AKNA foci with ODF2, DCTN1, EB1, dynein and CAMSAP3 ($n = 2$ experiments; 4 experiments for CAMSAP3). **f**, Co-immunoprecipitation experiments with lysates from E14 cerebral cortex, immunoprecipitation with AKNA antibody and western blot with AKNA, ODF2, DCTN1, EB1 AND GCP2, showing that these proteins are in the same complex, except GCP2 (that is, γTuRC) ($n = 2$ independent experiments for each). Scale bars, 5 μm (**a–e**).
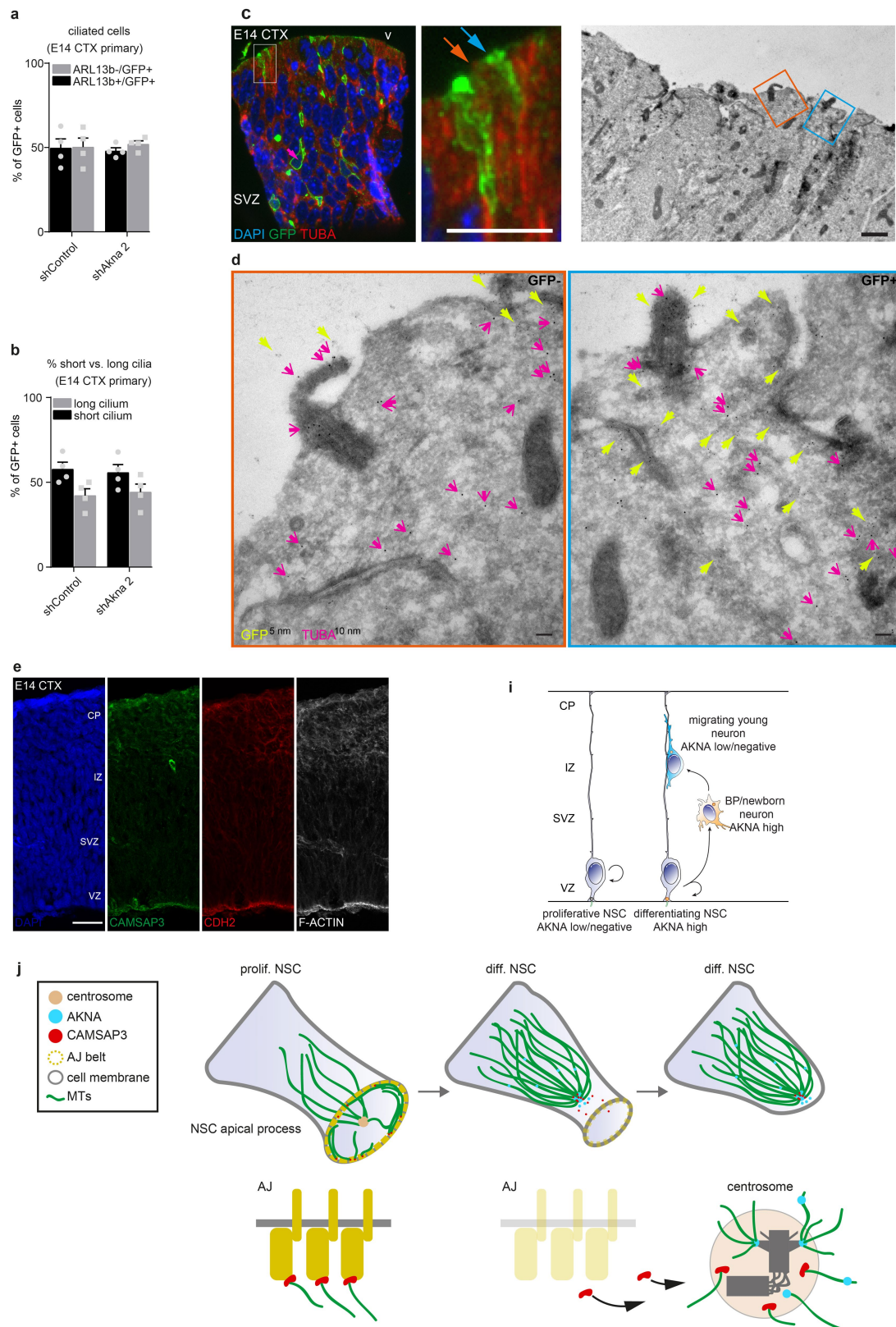
Extended Data Fig. 7 | See next page for caption.

Extended Data Fig. 7 | AKNA effects on cilia formation or localization, the upstream regulation of *Akna*, and summary of AKNA effects.
a, b, Histograms depicting the percentages of ciliated cells (ARL13^{+})
(**a**, $n = 4$ independent experiments) and short versus long cilia (**b**, $n = 4$ independent experiments), in E14 primary cortical cells transfected with control shRNA or *Akna* shRNA. Short cilia are defined as dot-like (short axoneme or cilium not fully exposed to cell surface), and long cilia are defined as rod-shaped (long axoneme exposed at the cell surface).
c, d, Integrated correlative light and electron microscopy micrographs of in utero-electroporated cells ($n = 2$ embryos). The images compare two neighbouring NSCs; one electroporated (blue) and one non-electroporated

(orange). Yellow and pink arrows show anti-GFP and anti-TUBA immunogold signal in the cytoplasm and cilium of the electroporated cell. Notice that AKNA electroporation does not notably affect cilia formation in vivo. **e**, Confocal micrographs of CAMSAP3, CDH2 (N-cadherin) and F-actin staining in E14 cortex. **i**, Model describing the expression and functional role of AKNA in delamination and seeding of the SVZ.
j. Schematic indicating and summarizing the modes of AKNA function in NSC delamination. Data in **a, b** are presented as mean ± s.e.m. Scale bars, 30 μm (**c**, immunofluorescence), 1 μm (**c**, electron microscopy), 0.1 μm (**d**), 25 μm (**e**).
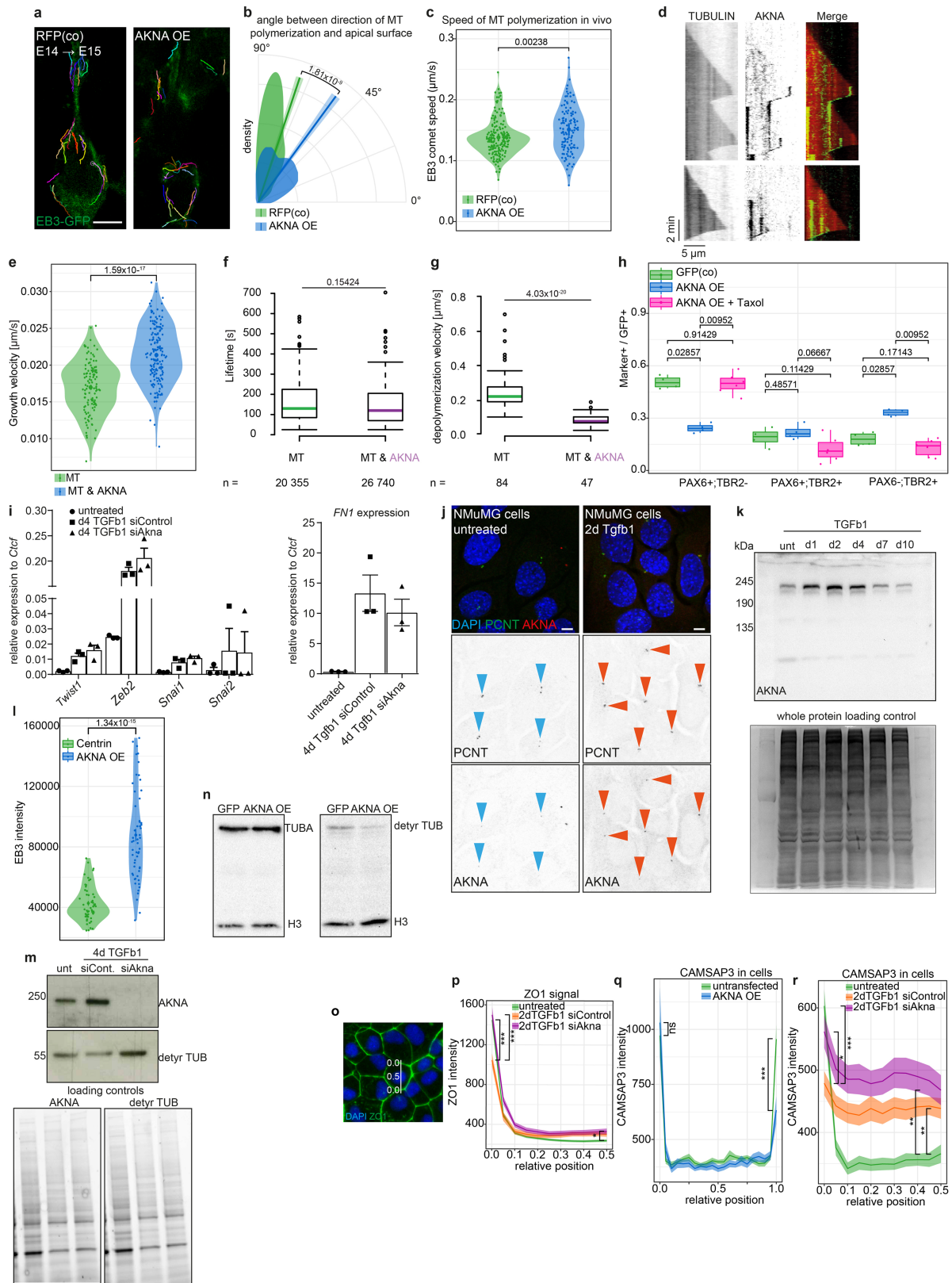
Extended Data Fig. 8 | See next page for caption.

Extended Data Fig. 8 | CAMSAP3 in the developing cortex, AKNA binding to and effects on purified microtubules, and AKNA regulation and function during EMT in mammary epithelial cells. a–c, AKNA overexpression in E14 cortex influences both the orientation (**a**, **b**, control, 117 EB3-comets; AKNA overexpression, 122 EB3-comets in 3 experiments; plot shows the distribution and solid line indicates the mean, ± s.e.m. as transparent band) and speed (**c**, control, 178 EB3-comets; AKNA overexpression, 113 EB3-comets) of microtubule polymerization monitored by live imaging of EB3–GFP in cortical slices 1 day after IUE. **d,** Representative kymographs obtained from TIRF time-lapse images of microtubules assembled in vitro from bovine brain tubulin labelled with Cy5 in the presence of AKNA–GFP. Cy5 is shown in red and GFP in green. **e–g,** Dynamic instability parameters of microtubules assembled from bovine brain tubulin with and without AKNA. Tubulin concentration was 15 μM and AKNA concentration was 75 ng ml^{-1}. In reactions containing AKNA, the growth velocity was increased. Moreover, the mean depolymerization velocity of shrinking plus ends without an AKNA signal was 0.27 μm s^{-1}, and the mean velocity was 0.10 μm s^{-1} when AKNA was associated with the plus end (**g**). **e, f,** Microtubule, $n = 117$; microtubule and AKNA, 174; **g,** microtubule, $n = 84$; microtubule and AKNA, $n = 47$ single measurements made from 2 (microtubule) and 3 (microtubule and AKNA) independent experiments. **h,** Box plot showing marker expression 24 h after IUE of GFP (control) ($n = 4$ embryos), AKNA overexpression ($n = 4$ embryos) and AKNA overexpression supplemented with Taxol (20 μM) ($n = 6$ embryos). GFP (control) and AKNA overexpression is the same data as shown in Fig. 1j. Note that the addition of Taxol during IUE rescues the phenotype of AKNA overexpression. **i,** Bar graph illustrating the mRNA expression of *Twist1, Zeb2, Snai1, Snai2* and *Fn1* by qRT–PCR ($n = 3$ individual experiments) after TGFβ1 treatment and siRNA transfection (data are shown as mean ± s.e.m.). **j,** AKNA immunofluorescence in untreated and TGFβ1-treated (two-day treatment) NMuMG cells. Red arrows indicate AKNA^{-} centrosomes (PCNT^{+}) in untreated cells, and blue arrows indicate AKNA^{+} centrosomes in TGFβ1-treated cells.

k, Western blot showing AKNA protein increase during the first days after EMT induction, and subsequent decrease to levels similar to those in untreated cells. Coomassie-stained gel showing equal loading is shown below. **l,** Dot and violin plot depicting the EB3–GFP fluorescence intensity measured at the centrosome in control (Centrin–tdTomato) and AKNA–mKO2 overexpression NMuMG cells, indicating the increased centrosomal microtubule nucleation after AKNA overexpression (GFP, 57 cells; AKNA overexpression, 56 cells). **m,** Western blot of AKNA and de-tyrosinated tubulin in untreated cells, and in cells transfected with control and *Akna* siRNA after four days of TGFβ1 treatment. Note the efficient knock down of AKNA by siRNA treatment, and the concomitant increase in detyrosinated tubulin. Whole protein detection illustrating equal protein loading is shown below. **n,** Western blot of TUBA and detyrosinated tubulin in control (GFP) and AKNA overexpression-transfected NMuMG cells 12 h after transfection. Note the decrease in detyrosinated tubulin upon AKNA overexpression. **o,** Micrograph illustrating how the quantification for ZO-1 was performed in **p. p,** Line graph depicting the quantification of ZO-1 intensity profiles across cells along white lines (see also Fig. 3a) (untreated, $n = 60$ cells; TGFβ1-treated, control siRNA, $n = 55$ cells; TGFβ1-treatment, *Akna* siRNA, $n = 76$ cells; cell junctions = position 0). *$P \leq 0.05$, **$P \leq 0.01$, ***$P \leq 0.001$ (exact P values (from left to right) 5.2×10^{-6}, 0.00004 and 0.04177). **q,** Line graph depicting the quantification of CAMSAP3 intensity profiles across cells, as indicated in Fig. 3e (untransfected, $n = 26$ cells; AKNA overexpression, $n = 22$ cells). NS, not significant, ***$P \leq 0.001$ (exact P values (from left to right) 0.53142 and 0.00003). **r,** Line graph depicting the quantification of CAMSAP3 intensity profiles across cells, as in Fig. 3e (untreated, $n = 42$ cells, TGFβ1-treated and control siRNA, $n = 51$ cells; TGFβ1-treated and *Akna* siRNA, $n = 50$ cells). *$P \leq 0.05$, ***$P \leq 0.001$ (exact P values (from left to right) 0.02478, 0.00038, 0.00095 and 0.00086). **f–h,** Box plots show median, quartiles (box) and range (whiskers). **c, e, l,** Violin plots show distribution of individual measurements (dots) with mean ± s.e.m. in bold in the centre (two-sided Mann–Whitney U test). Scale bars, 5 μm (**j**), 25 μm (**a**).
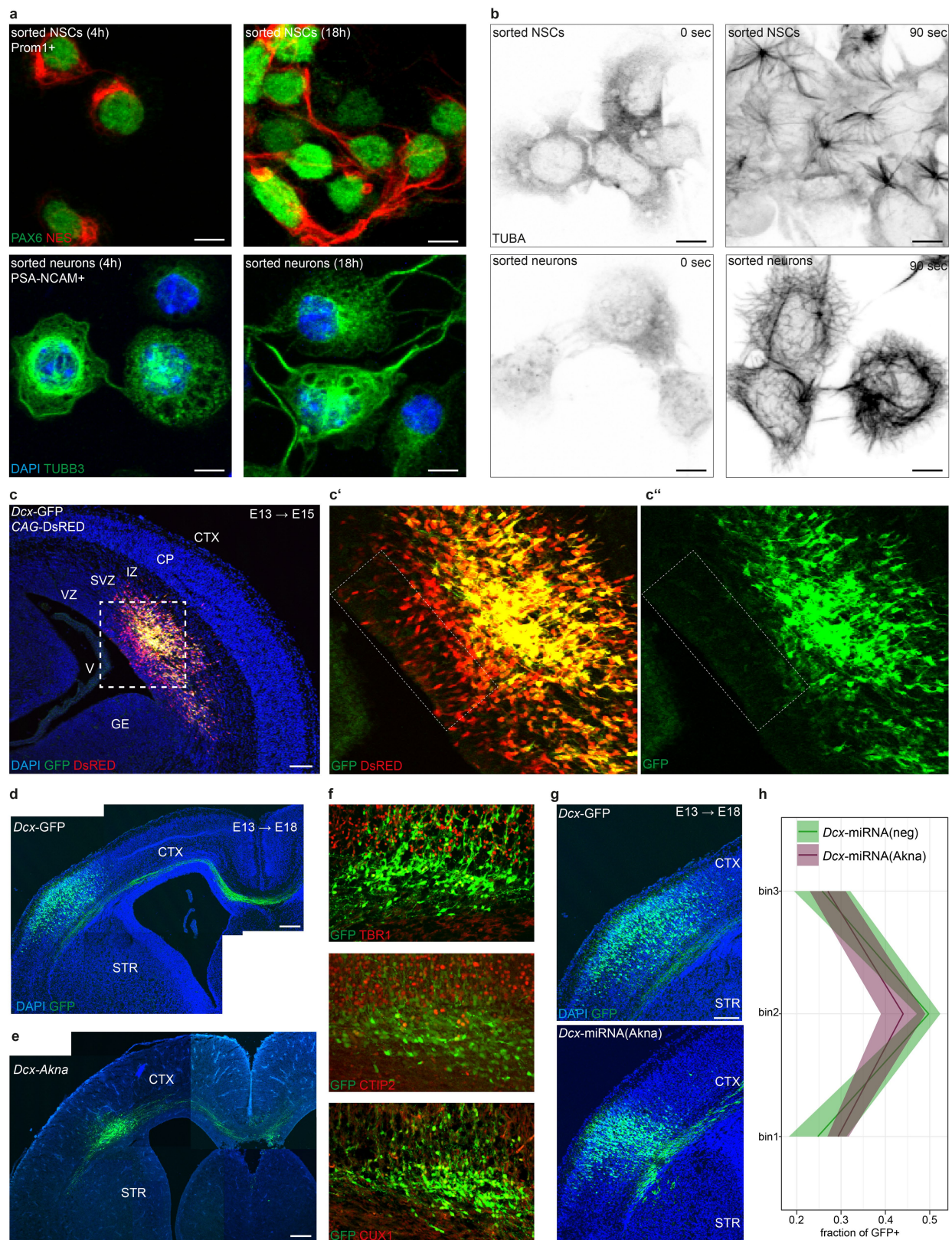
Extended Data Fig. 9 | See next page for caption.

Extended Data Fig. 9 | Lower levels of AKNA in differentiating neurons mediate non-centrosomal microtubule polymerization and allow migration into the cortical plate. a, **b**, Primary E14 cortical cells were sorted for PROMININ 1 (CD133) to isolate NSCs or for PSA-NCAM to isolate neurons as indicated in the panels. PROM1$^+$ cells express the NSC marker nestin, whereas PSA-NCAM$^+$ cells express the neuronal marker TUBB3, showing the specificity of the FACS (**a**) ($n = 2$ independent experiments). Microtubule regrowth assay in purified NSCs shows centrosomal microtubule polymerization (**b**, top), and purified neurons show largely non-centrosomal microtubule polymerization patterns (**b**, bottom) ($n = 2$ independent experiments). **c**, Micrographs showing co-electroporation of a CAG–dsRED and DCX–GFP at E13 and analysis at E15. Note the onset of *Dcx*–GFP expression (**c″**) only in the SVZ and cortical plate of the developing cortex, whereas DsRED$^+$ cells are also found in the ventricular zone (**c**, **c′**) ($n = 3$ embryos). **d**, **e**, Micrographs showing electroporated cells (GFP$^+$) in control (*Dcx*-GFP) (**d**) and *Akna* overexpressing (*Dcx-Akna*) (**e**) conditions ($n = 3$ embryos each conditions). Note that many AKNA overexpression cells accumulate in the SVZ, and are unable to migrate into the cortical plate. **f**, Micrographs of AKNA overexpression cells retained in the SVZ co-stained for TBR1, CTIP2, AND CUX1, which label neurons of different layer identity ($n = 3$ embryos). Note that the neuronal populations accumulating below the cortical plate upon *Dcx*-driven *Akna* expression contain neurons that are positive for each of these neuronal identities. **g**, Micrographs showing that electroporated cells (GFP$^+$) after control and *Dcx*-driven miRNA mediated downregulation of AKNA enter the cortical plate equally well ($n = 3$ embryos). **h**, Line graph illustrating the distribution of GFP$^+$ cells after IUE for *Dcx*-miRNA(neg), and *Dcx-Akna* miRNA no. 4. Mean ± s.e.m. as a transparent band (*Dcx*-miRNA(neg), $n = 4$; *Dcx-Akna* miRNA no. 4, $n = 3$ embryos). Scale bars, 5 μm (**a**, **b**), 50 μm (**c–g**).
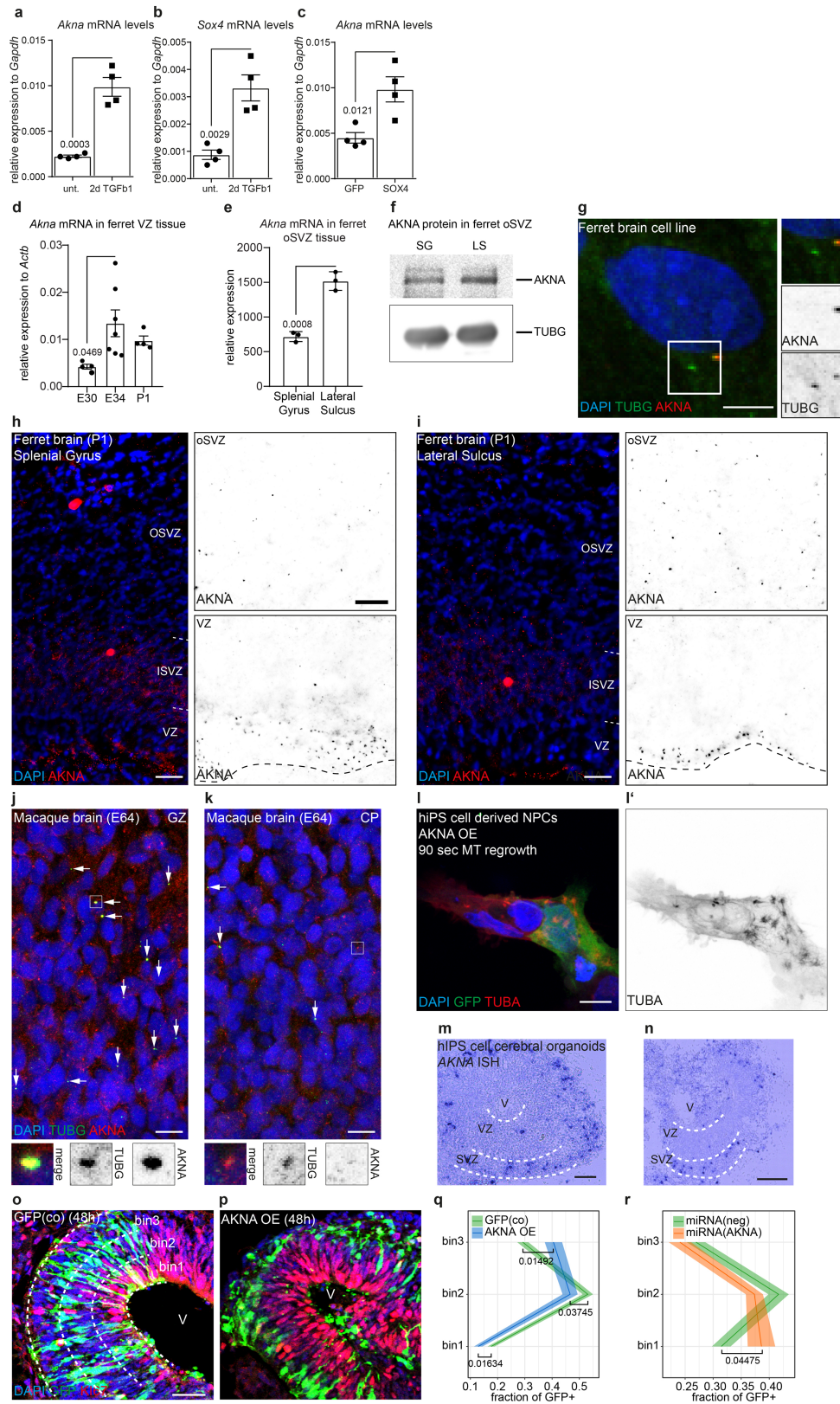
Extended Data Fig. 10 | See next page for caption.

Extended Data Fig. 10 | AKNA localization in ferret and macaque cerebral cortex and function in human cerebral cortex organoids.
a, **b**, RT–qPCR of *Akna* and *Sox4* in untreated or TGFβ1-treated NMuMG cells (treated for two days) showing upregulation during EMT ($n = 4$ independent experiments, mean ± s.e.m.). **c**, RT–qPCR of *Akna* after SOX4 overexpression in N2A cells for 36 h ($n = 4$ independent experiments, mean ± s.e.m.). **d**, qRT–PCR for *Akna*, showing the transient but strong upregulation of *Akna* mRNA in ferret ventricular zone tissue at E34—the time at which cells that form the outer SVZ (oSVZ) leave the ventricular zone[32] ($n = 4$ (E30), 7 (E34), 4 (P1) biologically independent samples). **e**, **f**, Microarray[33] ($n = 3$ biologically independent samples) (**e**) and western blot (**f**, 3 independent experiments) data showing higher levels of AKNA in the lateral sulcus (LS) compared to splenial gyrus (SG) in the oSVZ tissue of ferret brain at P1. **g**, Micrograph showing AKNA and TUBG co-localization at centrosomes in ferret brain cells (3 independent experiments). **h**, **i**, Comparison of AKNA immunofluorescence in ferret ventricular zone and oSVZ tissue in splenial gyrus versus lateral sulcus. Note the more-abundant immunofluorescence signal in the oSVZ of the lateral sulcus, corresponding with mRNA and protein levels as determined by western blot ($n = 2$ biologically independent samples). Given that the oSVZ of the gyrus contains more basal radial glia with bipolar morphology than does that of the sulcus, we propose that AKNA levels regulate the multipolar-to-bipolar transition in ferret SVZ, as AKNA levels do in mouse SVZ, with higher levels of AKNA leading to the retention of more cells in a multipolar state (see Fig. 4g–j). **j**, **k**, AKNA immunofluorescence in developing macaque germinal zone (GZ) and cortical plate ($n = 2$ sections from 2 animals). Arrows indicate AKNA+ centrosomes and denote abundant immunofluorescence signal. The square in **j** shows a representative example of a TUBG+AKNA+ centrosome in the germinal zone, and the square in (**k**) depicts an AKNA− centrosome in the cortical plate. **l**, Micrographs of human NPCs derived from hiPSCs that overexpress AKNA, showing multiple foci of microtubule polymerization ($n = 2$ independent experiments). **m**, **n**, In situ hybridization in hiPSC-derived cerebral organoids showing enrichment of *Akna* mRNA in non-apical SVZ-like areas (representative images of ventricular-zone-like structures from organoids of two independent culture batches). **o**, **p**, Micrographs showing sections of human brain organoids stained for GFP+ cells, electroporated with a control plasmid (**o**) or a plasmid overexpressing human *AKNA* cDNA (**p**). **q**, Line graph illustrating the distribution of GFP+ cells after IUE for GFP and AKNA overexpression (GFP, $n = 36$ ventricular zones; AKNA overexpression, $n = 37$ ventricular zones out of 2 independent organoid culture batches). **r**, Line graph illustrating the distribution of GFP+ electroporated cells after IUE for control miRNA and *Akna* miRNA knock down (control miRNA, $n = 36$ ventricular zones; *Akna* miRNA, $n = 31$ ventricular zones out of 2 independent organoid culture batches). **q**, **r**, Line graphs show mean ± s.e.m. as transparent band in the same colour. **a**–**c**, **e**, Two-sided Students *t*-test; **d**, one-way ANOVA followed by Tukey's post hoc test; **q**, **r**, two-sided Mann–Whitney *U* test. Scale bars, 5 μm (**g**), 50 μm (**h**, **i**, **m**, **n**), 10 μm (**l**, **j**, **k**).

32. Martínez-Martínez, M. A. et al. A restricted period for formation of outer subventricular zone defined by Cdh1 and Trnp1 levels. *Nat. Commun.* **7**, 11812 (2016).

33. de Juan Romero, C., Bruder, C., Tomasello, U., Sanz-Anquela, J. M. & Borrell, V. Discrete domains of gene expression in germinal layers distinguish the development of gyrencephaly. *EMBO J.* **34**, 1859–1874 (2015)

nature research

Corresponding author(s): Magdalena Götz

Last updated by author(s): Jan 10, 2019

Reporting Summary

Nature Research wishes to improve the reproducibility of the work that we publish. This form provides structure for consistency and transparency in reporting. For further information on Nature Research policies, see Authors & Referees and the Editorial Policy Checklist.

Statistics

For all statistical analyses, confirm that the following items are present in the figure legend, table legend, main text, or Methods section.

n/a	Confirmed	
☐	☒	The exact sample size (*n*) for each experimental group/condition, given as a discrete number and unit of measurement
☐	☒	A statement on whether measurements were taken from distinct samples or whether the same sample was measured repeatedly
☐	☒	The statistical test(s) used AND whether they are one- or two-sided *Only common tests should be described solely by name; describe more complex techniques in the Methods section.*
☐	☒	A description of all covariates tested
☐	☒	A description of any assumptions or corrections, such as tests of normality and adjustment for multiple comparisons
☐	☒	A full description of the statistical parameters including central tendency (e.g. means) or other basic estimates (e.g. regression coefficient) AND variation (e.g. standard deviation) or associated estimates of uncertainty (e.g. confidence intervals)
☐	☒	For null hypothesis testing, the test statistic (e.g. *F*, *t*, *r*) with confidence intervals, effect sizes, degrees of freedom and *P* value noted *Give P values as exact values whenever suitable.*
☒	☐	For Bayesian analysis, information on the choice of priors and Markov chain Monte Carlo settings
☒	☐	For hierarchical and complex designs, identification of the appropriate level for tests and full reporting of outcomes
☒	☐	Estimates of effect sizes (e.g. Cohen's *d*, Pearson's *r*), indicating how they were calculated

Our web collection on statistics for biologists contains articles on many of the points above.

Software and code

Policy information about availability of computer code

Data collection	Movies and immunofluorescence images: Olympus FV1000 confocal laser-scanning microscope FV 4.2, DeltaVision Core system, LEICA DM 6000 CS SP5 system LAS X 3.4, Leica SP8X STED 3D DLS LAS X 3.4, Axioplan2 epifluorescence microscope (Zeiss) Zen 2.0, Nikon A1 confocal microscope, Zeiss Super Resolution LSM880 AiryScan Elyra S1 Zen 2.3, Zeiss Z1 Axio Observer microscope with Yokogawa CSU-X1 spinning disk unit Zen 2.0, motorized inverted Nikon Eclipse Ti-E microscope with a motorized TIRF angle . Electron Microscopy: Morgagni EM at 80 kV (FEI) with a Morada camera. Western blots: Curix 60 (AGFA) with ECL method on Röntgen films (Fujifilm), ChemiDoc XRS (BioRad, 5.2.1). Mass spectrometry: Q Exactive high field mass spectrometer (Thermo Fisher) coupled to a RSLC HPLC system (Ultimate 3000, Thermo Fisher). FACS: Aria Cell Sorters (BD Biosciences, FACSDiva 6.1.3)
Data analysis	R Studio (1.1.456), R (3.5.1), GraphPad Prism (7.04), Python (3.6.5). Movies and IF: Fiji/ImageJ (2.0), ND acquisition software (Nikon), Picasso software suite (0.2.4; Endesfelder et al., 2014, 10.1007/s00418-014-1192-3), Imaris Software (Bitplane, 8.2), Huygens Software (SVI, 14.8-14.10), Leica LAS X 3.4. EM: ITEM software (EMSIS, 5.1 build 2677). WB: Image Lab Software (BioRad 5.2.1). MS: Progenesis QI software (Nonlinear, Waters, 2.5), Mascot (MatrixScience, London, UK; version 2.5.1) with Ensembl mouse public database, FACS: BD FACSDiva (6.1.3) and Flowjo (10.2) software

For manuscripts utilizing custom algorithms or software that are central to the research but not yet described in published literature, software must be made available to editors/reviewers. We strongly encourage code deposition in a community repository (e.g. GitHub). See the Nature Research guidelines for submitting code & software for further information.

Data

Policy information about [availability of data](#)

All manuscripts must include a [data availability statement](#). This statement should provide the following information, where applicable:

- Accession codes, unique identifiers, or web links for publicly available datasets
- A list of figures that have associated raw data
- A description of any restrictions on data availability

> The datasets generated in this study have been made available as Supplementary Information (and Supplementary Table 2). Further data are available upon reasonable request from the corresponding author.

Field-specific reporting

Please select the one below that is the best fit for your research. If you are not sure, read the appropriate sections before making your selection.

☒ Life sciences ☐ Behavioural & social sciences ☐ Ecological, evolutionary & environmental sciences

For a reference copy of the document with all sections, see [nature.com/documents/nr-reporting-summary-flat.pdf](#)

Life sciences study design

All studies must disclose on these points even when the disclosure is negative.

Sample size	No statistical methods were used to predetermine sample sizes. Sample size were predetermined on the basis of published studies. All quantitative experiments in this study were repeated at least three times. For in vivo experiments the number of embryos subjected to a particular experiment are defined by the number of embryos available in the mice operated and the statistical requirements.
Data exclusions	No samples, no animals and no data was excluded
Replication	All experiments in this study, except the proteomic analysis in Extended Data Fig. 1o, were replicated multiple times with the same experimental protocol, followed by the same analysis. All replications were successful and showed the same results.
Randomization	All animals, human cerebral organoids and wells of cultured cells were assigned to groups randomly
Blinding	Blinding was not possible, due to the very strong phenotype after Akna manipulation (see Fig. 1, 2 ,4). Quantifications in Fig. 3 were analysed in a blinded manner.

Reporting for specific materials, systems and methods

We require information from authors about some types of materials, experimental systems and methods used in many studies. Here, indicate whether each material, system or method listed is relevant to your study. If you are not sure if a list item applies to your research, read the appropriate section before selecting a response.

Materials & experimental systems

n/a	Involved in the study
☐	☒ Antibodies
☐	☒ Eukaryotic cell lines
☒	☐ Palaeontology
☐	☒ Animals and other organisms
☒	☐ Human research participants
☒	☐ Clinical data

Methods

n/a	Involved in the study
☒	☐ ChIP-seq
☐	☒ Flow cytometry
☒	☐ MRI-based neuroimaging

Antibodies

Antibodies used	Commercial primary antibodies are: Akna (DSHB, clone 1C7, mouse, 1:25), Arl13b (ProteinTech 17711-1AP, rabbit, 1:200, lot 00040297), Actb (C4) (Santa Cruz sc-47778, mouse, 1:1000, lot F1417), CAMSAP2 (ProteinTech 17880-1-AP, rabbit, lot 00009360), Cdh2/N-Cadherin (BD Transduction Laboratories 610921, mouse, clone 32/N-Cadherin, 1:250, lot 46226), Clasp2 (Millipore ABT263, rabbit, 1:200, 3040386), Cep170 (Novus NB100-55317, rabbit, 1:200, lot A1), Ckap5 (H4) (Santa Cruz sc-374394, mouse, 1:50, lot G0716), Ctip2 (Abcam ab18465, rat, clone 25B6, 1:250, lot GR243609-2), Cux1/CDP (M-222) (Santa Cruz sc-13024, rabbit, 1:50 to 1:500, lot F0315), CyclinD1 (Thermo Fisher RM9104R7, rabbit, 1:500, lot 910R1107C), Dynein IC (Millipore, MAB1618, mouse, clone 74.1, 1:100 to 1:500, lot 2876150), Dctn1 (H-300) (Santa Cruz sc-11363, rabbit, 1:50 to 1:500, lot F2609), Dctn1/p150Glued (BD Transduction Laboratories 612709, mouse, Clone 12/P150GLUED, 1:100 to 1:1000, lot 5192749), Dctn2 (H-300) (Santa Cruz sc-135135, rabbit, 1:500, lot F2410), Dctn4 (Abcam ab170107, rabbit, 1:500 to 1:2000, lot YJ121404DS), Dcx (Millipore AB2253,

guinea pig, 1:1000, lot 2787730), EB1 (H-70) (Santa Cruz sc-8356, rabbit, 1:50 to 1:1000, lot K1709), E-Cadherin (DECMA-1) (Abcam ab11512, rat, 1:500, lot GR3215680-2), FLAG – M2 (Sigma F1804, mouse, 1:500, lot SLBN2445V), Gapdh (Millipore MAB374, mouse, clone 6C5, 1:1000 to 1:3000, lot NG1722294), GCP2 (Novus NBP2-21793, mouse, clone GCP2-01, 1:500, lot 525992), GCP2 (F3) (Santa Cruz sc-377117, rabbit, 1:500, lot AS2114), GCP4 (D-5) (Santa Cruz sc-271876, rabbit, 1:100, lot B0414), GFP (Aves Lab GFP-1020, chicken, 1:1000, lot 0511FP12), GT335 (AdipoGen AG20B-0020, mouse, clone GT335, 1:2000, lot A20631002), Histone H3 (Abcam ab1791, rabbit, 1:1000 to 1:5000, lot GR2100231), Ki67 (Leica/Novocastra NCL-Ki67p, rabbit, 1:200, lot PA 0230 44924), Ki67 (Abcam ab92742, rabbit, clone EPR3610, 1:500, lot GR213055-34), Ki67 (Invitrogen/ Thermo Fisher 14-5698-82, rat, clone SolA15, 1:500, lot 2002315), NEDD1 (39-J) (Santa Cruz, sc-100961, mouse, 1:50 to 1:100, lot L2914), Nestin (Millipore MAB353, mouse, clone rat-401, 1:500, lot 2041569), NeuN (Millipore MAB377, mouse, clone A60, 1:500, lot 2549411), Odf2 (Abcam ab43840, rabbit, 1:200, lot GR127791-1), Odf2 (G-2) (Santa Cruz sc-393881, mouse, 1:50 to 1:500, lot A2414), Ctnnd1/p120 (Abcam ab92514, rabbit, 1:500, lot GR19086717), p53 (Cell Signaling 2524, mouse, clone 1C12, 1:500, lot 13), p-120 (Abcam ab81318, rabbit, 1:500, lot YF071003C), Pan-Cadherin (Sigma C3678, rabbit, 1:500, lot 093164870), Pax6 (Millipore AB2237, rabbit, 1:500, lot 2910153), Pax6 (DSHB AB 528427, mouse, 1:25, home-made hybridoma sypernatant), PCNA (DAKO M0879, mouse, clone PC10, 1:500, lot 00083603), Pcnt (Biolegend 923701, rabbit, 1:500, lot B200667), Phalloidin-Atto 647N (Sigma, 65906, lot BCBW3497), p-Histone H3 (Ser10) (Millipore 06-570, rabbit, 1:500, lot 2517793), RFP (Rockland 600401379, rabbit, 1:500, lot 35055), Tbr1 (Abcam ab31940, rabbit, 1:200, lot GR204561), Tbr2 (Millipore AB15894, chicken, 1:500, lot 2391191), Tbr2 (Abcam ab23345, rabbit, 1:250, lot GR153320-1), Tbr2 (Abcam ab183991, rabbit, clone EPR19012, 1:500, lot GR2883504), Tuba (Sigma T5168, mouse, clone B-5-1-2, 1:1000 to 1:20,000, lot 103M4773V), Tuba (Thermo Fisher MA1-80017, rat, 1:200), Tubb3 (Sigma T8660, mouse, clone SDL.3D10, 1:1000, lot 103M4830), Tubg (Sigma T6557, mouse, clone GTU-88, 1:250, lot 070M4856), Tubg (Sigma T5192, rabbit, 1:200, lot 109K4802), Tubg (ProteinTech 15176-1-AP, rabbit, 1:200, lot2578104), Tubulin acetylated (Sigma T7451, mouse, clone 6-11b-1, 1:2000, lot 103M4772V), Tubulin tyrosinated (Sigma MAB1864-I, rat, clone YL1/2, 1:5000, lot GR3187372-2), Tubulin detyrosinated (Millipore AB3201, rabbit, 1:1000, lot 2886375), ZO-1 (Invitrogen 617300, rabbit, 1:500 to 1:2500, lot SH252320). For flow cytometry PSA-NCAM PE-coupled (Miltenyi 130-093-274, mouse, clone 2-2B, 1:750, lot 5150810207) and CD133 APC-coupled (eBioscience 17-1331, rat, clone 13A5, 1:500, lot 4290710) were used.

Commercial secondary antibodies are:
mouse IgG HRP (Invitrogen 62-6520, goat, 1:10,000, lot SI257293), rat IgG HRP (Ge Healthcare Life Sciences NA935, goat, 1:5000, lot 9700734), rabbit IgG HRP (Ge Healthcare Life Sciences NA934-1ML, donkey, 1:10,000, lot 16885523), mouse IgG HRP (Rockland 18-8817-30, rat, 1:1000, lot 32642), rabbit IgG HRP (Rockland 18-8816-31, mouse, 1:1000, lot 34665), goat IgG HRP (Chemicon AP106p, rabbit), rat unconjugated (Jackson ImmunoResearch/Dianova 712-005-150, donkey), chicken A488 (Thermo Fisher A11039, goat, lot 1637891), chicken A546 (Thermo Fisher A11040, goat, 1094435), rat A488 (Thermo Fisher A11006, goat, lot 1689880), rat A546 (Thermo Fisher A11081, goat, lot 1661229), rat A647 (Thermo Fisher A21247, goat, lot 16543056), rabbit A488 (Thermo Fisher A11008, goat, lot 1735088), rabbit FAB 488 (Jackson ImmunoResearch 711-547-003 donkey, lot 128821), rabbit A546 (Thermo Fisher A11010, goat, lot A11010), rabbit A568 (Thermo Fisher A11011, goat), rabbit A633 (Thermo Fisher A21070, goat, lot 1739295), rabbit A647 (Thermo Fisher A21244, goat, lot 1696456), guinea pig A488 (Thermo Fisher A11073, goat, lot 52959A), guinea pig A546 (Thermo Fisher A11074, goat, lot 1716235), mouse IgG A488 (Thermo Fisher A11029, goat, lot 1306597), mouse IgG1 A488 (Thermo Fisher A21121, goat, lot 719913), mouse IgG1 A546 (Thermo Fisher A21123, goat, lot 1722393), mouse IgG1 A647 (Thermo Fisher A21240, goat, lot 1661240), mouse IgG2a A488 (Thermo Fisher A21131, goat, lot 1145164), mouse IgG2a A546 (Thermo Fisher A21133, goat, lot 1694115), mouse IgG2b A488 (Thermo Fisher A21141, goat, lot 1512106), mouse IgG2b A546 (Thermo Fisher A21143, goat, lot 1711516), rabbit AS635P (Abberior 2-0012-007-2, goat, 1:200, lot 18012016HP), mouse IgG AS580 (Abberior 2-0002-005-1, goat, 1:200, lot 22012016CW). *A = Alexa Fluor; ** AS = Abberior Star. Unless otherwise described, fluorencent labelled secondary antibodies were used at a dilution of 1:500 to 1:1000. HRP-coupled secondary antibodies were used at a dilution of 1:5000 to 1:10,000.

Isotypes controls are:
IgG1 isotype (Biolegend 401402, mouse, clone MG1-45, lot B197935), normal IgG (Santa Cruz sc-2027, rabbit, lot H2615), IgM isotype PE (Miltenyi 130093177, mouse, clone IS5-20C4, 1:750, lot 5170328287), IgG1 isotype APC (eBioscience 17-4301, rat, clone eBRG1, 1:500, lot E07258-1632)

Home-made antibodies are: Akna (25F1, mouse IgG1, IF (1:25-1:100)), Akna (14D7, rat IgG2a, WB (1:10), IF (1:25-1:100)), AKNA-A (9G1, rat IgG1, WB (1:10), IF (1:25-1:100)), AKNA-B (4F5, rat IgG2a), WB (1:10), IF (1:25-1:100)), HA (mouse IgG1, for IP used 1 ml supernatant), Camsap3 (kind gift of Masatoshi Takeichi, RIKEN CDB, Meng et al., 2008, 10.1016/j.cell.2008, rabbit, 1:100 to 1:500), Cas9 (8G1-1-1, rat IgG2a, WB (1:10)), Sox4 (kind gift of Elisabeth Sock, University of Erlangen-Nürnberg, Hoser et al.,2008, 10.1128/MCB.00338-08,, guinea pig, 1:2000)

Validation	Antibodies were validated by the manufacturer and corroborated with previously published antibody staining results. Home made antibodies were validated by immunofluoresence and/or Western Blot and RNAi.

Eukaryotic cell lines

Policy information about cell lines

Cell line source(s)	Neuro2A: Oskar Ortiz, Institute for Developmental Genetics, Helmholtz Center München, Germany (ACC 148, DSMZ, Braunschweig, Germany) NMuMG: Vijay Tiwari Institute for Molecular Biology, Mainz, Germany (clone NMuMG/E9, from ATCC-CRL-1636) human iPS cells: Micha Drukker, Institute for Stem Cell Research, Helmholtz Center München, Germany (line HMGU1) and the Universitätsklinikum Erlangen (Havlicek et al., 2013; 10.1093/hmg/ddt644) A20: Elisabeth Kremmer, Core Facility Monoclonal Antibodies, Helmholtz Center München, Germany (ATCC TIB-208) Mpf cells: Victor Borrell, Instituto de Neurociencias, Universidad Miguel Hernández (Mpf ATCC CRL-1656)
Authentication	iPS cells were authenticated after reprogramming by karyotyping. The cell lines Neuro2A, NMuMG, A20, Mpf were not authenticated.

Mycoplasma contamination	Human iPS cells and the human iPS cells derived cerebral organoids were tested negative for mycoplasma. The cell lines Neuro2A, NMuMG, A20, Mpf were not tested for mycoplasma.
Commonly misidentified lines (See ICLAC register)	No commonly misidentified cell line was used in this study.

Animals and other organisms

Policy information about studies involving animals; ARRIVE guidelines recommended for reporting animal research

Laboratory animals	Female and male mice were used at embryonic stages E9, E11, E13, E14, E15, E18. C57BL/6J and RjHan:NMRI mice at 2 to 12 months of age were bred and time mated in house, or purchased from Charles River or Janvier, and used as a source for embryonic brain tissue, for in utero electroporations or monoclonal antibody generation. 2 to 12 months of old Sas4fl/fl; p53fl/fl; Emx1Cre were generated by the Song-Hai Shi lab (Insolera et al., 2014, 10.1038/nn.3831) to produce E14 embryos. Lou/C rats were bred in house at the HMGU and used for monoclonal antibody generation (90-150 days old). Pregnant female pigmented ferrets (Mustela putorius furo) were obtained from Marshall Farms and embyos (E30, E34) or neonaltal (P1) animals were used for experiments. Embryos (E64) of pregnant female cynomolgus monkeys (Macaca fascicularis) were used to obtain embryonic macaque brain tissue as describe in the methods.
Wild animals	The study did not involve wild animals.
Field-collected samples	The study did not involve samples collected from the field.
Ethics oversight	Mice: all experimental procedures were performed in accordance with the regulations of the Helmholtz Center Munich, the Biomedical Center of the LMU, the MSKCC IACUC, and GIGA-Neurosciences University of Liège. Ferrets: all animals were treated according to Spanish and EU regulations, and experimental protocols were approved by the Universidad Miguel Hernández IACUC. Cynomolgus monkey (Macaca fascicularis): the cynomolgus monkey facility in this study and all experimental protocols were approved by the Animal Care and Use Committee CELYNE (C2EA#42). Surgical procedures and animal experimentation were in accordance with European requirements 2010/63/UE. Protocols C2EA42-12-11-0402-003 and APAFIS#3183 have been approved by the Animal Care and Use Committee CELYNE (C2EA #42)" iPS cells: The use of iPSCs was approved by the Ethics Commission of LMU (Ludwig-Maximilians-Universität München), with the association number 115-16. Lines were derived from male newborn foreskin fibroblasts (CRL-2522, ATCC) or from healthy patient fibroblasts obtained following Institutional Review Board approval no. 4120 and informed patient consent at the Movement Disorder Clinic at the Department of Molecular Neurology, University Clinic Erlangen, Germany.

Note that full information on the approval of the study protocol must also be provided in the manuscript.

Flow Cytometry

Plots

Confirm that:

☒ The axis labels state the marker and fluorochrome used (e.g. CD4-FITC).

☒ The axis scales are clearly visible. Include numbers along axes only for bottom left plot of group (a 'group' is an analysis of identical markers).

☒ All plots are contour plots with outliers or pseudocolor plots.

☒ A numerical value for number of cells or percentage (with statistics) is provided.

Methodology

Sample preparation	Cortices from E14 embryos were dissected removing the ganglionic eminence, the olfactory bulb, the hippocampal anlage and the meninges. Single cells wereincubated with an APC-conjugated Prominin-1 antibody (CD133, eBioscience) or PE-conjugated PSA-NCAM antibody (Miltenyi Biotec). Sorted cells were examined through plating and immunohistochemistry (fixation 2-4 hours after plating) which confirmed their expected NSC (Pax6 positive) and neuronal identity (βIII-Tubulin positive) and the purity of the sorting procedure.
Instrument	Cells were isolated on Aria Cell Sorters (BD Biosciences)
Software	Data were analized with BD FACSDiva and Flowjo software
Cell population abundance	N/A (see above)
Gating strategy	Gating parameters were determined by side and forward scatter to eliminate debris (P1 gate) and aggregated cells (P2 gate). PE- and APC conjugated isotype control (eBioscience, Miltenyi Biotec) stained cells were used to set the positive and negative gates for the stained populations (both set to include maximum 0.1% of non-fluorescent cells).

☒ Tick this box to confirm that a figure exemplifying the gating strategy is provided in the Supplementary Information.